

Electronic Supplementary information for

Vapor-Solid Synthesis of Monolithic Single-Crystalline CoP Nanowire Electrodes for Efficient and Robust Water Electrolysis

Wei Li,^a Xuefei Gao,^b Dehua Xiong,^a Fang Xia,^c Jian Liu,^b Wei-Guo Song,^b Junyuan Xu,^a
Sitaramanjaneya Mouli Thalluri,^a M. F. Cerqueira,^d Xiuli Fu^e and Lifeng Liu^{a,*}

^a *International Iberian Nanotechnology Laboratory (INL), Av. Mestre Jose Veiga, 4715-330 Braga (Portugal)*

^b *Beijing National Laboratory for Molecular Sciences, Institute of Chemistry, Chinese Academy of Sciences, 100190 Beijing (P. R. China)*

^c *School of Engineering and Information Technology, Murdoch University, Murdoch, West Australia 6150, Australia*

^d *Center for Physics, University of Minho, 4710-057 Braga, Portugal*

^e *State Key Laboratory of Information Photonics and Optical Communications, and School of Science, Beijing University of Posts and Telecommunications, Beijing 100876, P. R. China*

* Corresponding author.

E-mail: lifeng.liu@inl.int (L.F. Liu)

Fax: +351 253 140 119.

Contents

I. Experimental section

II. Supplementary Figures

Figure S1. SEM images of a bare Co foam.

Figure S2. SEM images, EDX spectra and XRD patterns of Co_xP_y -700 and Co_xP_y -800.

Figure S3. XPS spectra of the CoP NWs electrode.

Figure S4. Steady-state CV curves and integrated charges of the $\text{Co}^{2+} \leftrightarrow \text{Co}^{3+}$ redox peaks of the CoP NWs electrode and bare Co foam.

Figure S5. Electrochemical impedance spectroscopy (EIS) Nyquist plots of CoP NWs and CF.

Figure S6. Steady-state CV curves of the CoP NWs synthesized at 600 °C for 1 h in the presence of 8 and 16 g of red P.

Figure S7. Steady-state CV curves of the CoP NWs synthesized at 600 °C using 8 g red P for 1 and 6 h.

Figure S8. Steady-state CV curves and Tafel plots of the cobalt phosphide electrodes synthesized at 600 (CoP -600), 700 (Co_xP_y -700) and 800 °C (Co_xP_y -800).

Figure S9. Chronoamperometric (CA) profile of a pristine CoP NWs electrode synthesized at 600 °C for 1 h.

Figure S10. SEM images of the CoP NWs electrodes after the CA measurements.

Figure S11. EDX spectra of the pristine CoP NWs electrode and those after the CA measurements.

Figure S12. HAADF-STEM image and elemental maps for a single NW after the CA measurement for 20 s.

Figure S13. HAADF-STEM image and elemental maps for a single NW after the CA measurement for 5 min.

Figure S14. HAADF-STEM image and elemental maps for a single NW after the CA measurement for 30 min.

Figure S15. HAADF-STEM image and elemental maps for a single NW after the CA measurement for 3 h.

Figure S16. HRTEM, HAADF-STEM image and elemental maps for a single NW after the CA measurement for 6 h.

Figure S17. Raman spectra of the pristine CoP electrode and those after the CA measurements.

Figure S18. High-resolution XPS spectra of the CoP NWs electrode and those after the CA measurements.

Figure S19. Electrocatalytic performance of the as-obtained CoP NWs electrode for the HER in 1.0 M KOH.

Figure S20. The polarization curves and Tafel plots of the CoP NWs electrodes synthesized at various temperatures for the HER.

Figure S21. Energy efficiency of the CoP NWs, RuO₂||Pt-C and bare CF electrolyzers for overall water splitting in 1.0 M KOH solution as a function of current density.

Figure S22. XRD patterns of the pristine CoP NWs, CoP NWs cathode and in-situ oxidized CoP NWs anode after overall water splitting in 1.0 M KOH at 20 mA cm⁻² for 1000 h.

Figure S23. SEM images and EDX spectrum of the CoP NWs cathode after overall water splitting in 1.0 M KOH at 20 mA cm⁻² for 1000 h.

Figure S24. SEM images and EDX spectrum of the in-situ oxidized CoP NWs anode after overall water splitting in 1.0 M KOH at 20 mA cm⁻² for 1000 h.

III. Supplementary Tables

Table S1. Comparison of the electrocatalytic performance of the in-situ oxidized CoP NWs electrode for the OER to that of reported non-precious metal electrocatalysts.

Table S2. Comparison of the electrocatalytic performance of the CoP NWs electrode for the HER to that of non-precious metal electrocatalysts reported in the literature.

Table S3. Comparison of the catalytic performance of the CoP NWs || oxidized CoP NWs electrode pair for two-electrode overall water splitting to that of reported non-precious metal electrocatalysts and precious metal electrocatalysts.

IV. Estimation of energy efficiency of water electrolyzers

V. References

Experimental section

Chemicals and materials

Red phosphorous (P, $\geq 97.0\%$), potassium hydroxide pellets (KOH, $\geq 85\%$), hydrochloric acid (37 wt.%) and absolute ethanol were purchased from Sigma-Aldrich, and used as received without any further purification. Co foam (CF, 1.0 mm thick, 110 Pores Per Inch) was obtained from Hezhe Jiaotong Group, China. Deionized (DI) water from a Millipore system ($18.2\text{ M}\Omega\cdot\text{cm}$) was utilized for solution preparation and rinsing.

Fabrication of the self-supported CoP NWs electrodes.

A piece of Co foam (CF, $3 \times 4.5\text{ cm}^2$) was cleaned by ultrasonication in 6 M HCl for 10 min, subsequently thoroughly rinsed with DI water and ethanol, and finally dried under N_2 flow at room temperature. The clean CF was loaded into a ceramic boat, with *ca.* 8 g of red phosphorous placed 1 cm away from the CF in the upstream side. Afterwards, the ceramic boat was put into a tube furnace (Carbolite). The furnace was then purged with nitrogen (N_2 , 99.999%), heated to $600\text{ }^\circ\text{C}$ at a ramping rate of $10\text{ }^\circ\text{C min}^{-1}$, and maintained at this temperature for 1 h. Finally, the furnace was naturally cooled down to room temperature. The N_2 flow (500 sccm) was maintained throughout the whole process. The resultant foam was washed with DI water and ethanol, and subsequently dried under N_2 flow. By calculating the weight change of the foam before and after phosphorization, *ca.* 35% of bulk Co foam was consumed during this phosphorization process. The resultant cobalt phosphide nanowires foam under this condition was denoted as CoP NWs throughout the main text unless otherwise specified.

The CoP NWs can also be successfully obtained by increasing the reaction time to 6 h or loading more red P (e.g., 16 g) under similar conditions. This led to the formation of CoP NWs with similar

morphology and structure. To investigate the effect of phosphorization temperature on the electrocatalytic performance, the phosphorization was also carried out at 700 and 800 °C while keeping all other phosphorization conditioned unchanged (i.e., 8 g of red P, 1 h reaction time). The corresponding resultant electrodes were denoted as Co_xP_y-700 and Co_xP_y-800, respectively.

Characterization

All the samples were thoroughly rinsed prior to characterization. Scanning electron microscopy (SEM) characterization was conducted using a FEI Quanta 650 FEG microscope equipped with an INCA 350 spectrometer (Oxford Instruments) for energy dispersive X-ray spectroscopy (EDX). X-ray diffraction (XRD) measurements were carried out on an X'Pert PRO diffractometer (PANalytical) at 45 kV and 40 mA, using Cu K_α radiation ($\lambda = 1.541874 \text{ \AA}$) and a PIXcel detector. XRD data were collected using Bragg-Brentano configuration in the 2θ range of 25 – 90 ° with a scan speed of 0.01° s⁻¹. The XRD patterns were indexed and analyzed according to the International Centre for Diffraction Data (ICDD) PDF-4+ database using the HighScore software package (PANalytical). Transmission electron microscopy (TEM), high-resolution TEM (HRTEM), high-angle annular dark-field scanning transmission electron microscopy (HAADF-STEM) and EDX elemental mapping studies were performed on a probe-corrected transmission electron microscope operating at 200 kV (FEI Titan ChemiSTEM 80-200). X-ray photoelectron spectroscopy (XPS) data were acquired on an ESCALAB 250Xi X-ray photoelectron spectrometer (Thermo Scientific) using Al K_α radiation. Raman spectra were collected by using Witec Alpha 300R confocal Raman system. The Raman measurements were performed with 50× objective lens, a laser excitation wavelength of 532 nm with a power of 0.8 mW and 2 s acquisition time and 100 accumulations. The grating was 600 g mm⁻¹.

Electrochemical measurements

All electrochemical measurements were conducted at room temperature (*ca.* 25 °C) using a Biologic VMP-3 potentiostat/galvanostat in a typical three-electrode configuration for the HER and the OER tests or a two-electrode configuration for overall water splitting.

The HER performance was evaluated in H₂-saturated 1.0 M KOH aqueous solution using the as-fabricated CoP NWs foam as the working electrode and a saturated calomel electrode (SCE) as a reference. A foil of electrocatalytically inactive gold (0.1 mm, 99.99 %, Sigma-Aldrich), instead of Pt, was employed as the counter electrode to avoid any contamination from Pt. The SCE electrode was calibrated before each measurement in H₂-saturated 0.5 M H₂SO₄ solution using a clean Pt wire as the working electrode. Prior to each HER test, the electrolyte was deaerated by bubbling with mixed H₂/N₂ gas (1 atm, 5% H₂ in 99.995 % N₂) for 2 h. The bubbling was then kept throughout the whole experiment.

The OER performance was evaluated in a three-electrode configuration in O₂-saturated 1.0 M KOH solution using the as-fabricated CoP NWs foam as the working electrode, a calibrated SCE as a reference, and a clean Pt foil as the counter electrode. Prior to each OER test, the electrolyte was deaerated by bubbling with high-purity O₂ (1 atm, 99.9999 %) for 2 h, and the bubbling was subsequently maintained throughout the whole experiment.

Linear sweep voltammetry (LSV) was performed at a scan rate of 2 mV s⁻¹ to obtain the polarization curves. Unless stated otherwise, all potentials are reported versus reversible hydrogen electrode (RHE) by converting the potentials measured vs. SCE according to the following equation:

$$E(\text{RHE}) = E(\text{SCE}) + 0.241 + 0.059 \times \text{pH} \quad (1)$$

The current density (j) presented in this work is normalized with respect to the geometric surface area of the electrode. No pre-activation (e.g., repetitive cyclic voltammetry) process was performed before the HER. For the CoP NWs electrode, the steady-state LSV curves can be obtained from the second scan for the HER. For the OER, the CoP NWs electrode was scanned by using cyclic voltammetry (CV) at 2 mV s^{-1} between 0.8375 V and 1.6375 V vs. RHE for 10 continuous cycles. Afterwards the steady-state CV curves can be obtained.

Accelerated degradation test (ADT) for the HER was performed using cyclic voltammetry (CV) at 50 mV s^{-1} in the range of $-0.22 - 0.2 \text{ V}$ vs. RHE for 1000 continuous cycles. To evaluate the long-term stability of the activated CoP NWs electrodes, chronopotentiometric (CP) measurements were carried out at a given constant current density. To investigate the conversion process of CoP to CoOOH, chronoamperometric (CA) measurements were carried out using pristine CoP NWs electrodes at the anodic potential of 1.54 V (non iR -corrected). Electrochemical impedance spectroscopy (EIS) measurements were carried out in the frequency range of $2 \times 10^5 - 5 \times 10^{-3} \text{ Hz}$ with 10 mV sinusoidal perturbations. Unless stated otherwise, all polarization curves measured in a three-electrode configuration are iR -corrected. The correction was made according to the following equation:

$$E_{\text{corr}} = E_{\text{mea}} - iR_c \quad (2)$$

where E_{corr} is iR -corrected potential, E_{mea} experimentally measured potential, and R_c is the compensated resistance measured by using the Bio-Logic EC-Lab software (ZIR technique).

For comparison, the electrocatalytic performance of a bare Co foam (CF), commercially available RuO_2 nanopowders (99.9%, Alfa Aesar) and Pt-C catalysts (20 wt.% Pt on Vulcan,

FuelCell Store) supported on CF (loading mass = 3.0 mg cm^{-2}) was also measured under the similar conditions.

For overall water splitting, a symmetrical full electrolyzer was constructed using two identical CoP NWs electrodes as cathode and anode, respectively. Overall water splitting performance was evaluated using LSV and CP in a two-electrode configuration in 1.0 M KOH. LSV curves were recorded at a sweep rate of 2 mV s^{-1} . The CP curves measured in a two-electrode configuration are not iR -corrected. For comparison, the control electrolyzers consisting of two identical Co foams or a pair of RuO_2 (anode) and Pt-C (cathode) catalysts loaded on the Co foams with the loading mass of 3.0 mg cm^{-2} were also tested under the above-mentioned conditions. Long-term stability of the two-electrode CoP NWs electrolyzer was evaluated by CP at 20 mA cm^{-2} and 100 mA cm^{-2} in 1.0 M KOH aqueous solution.

Supplementary Figures:

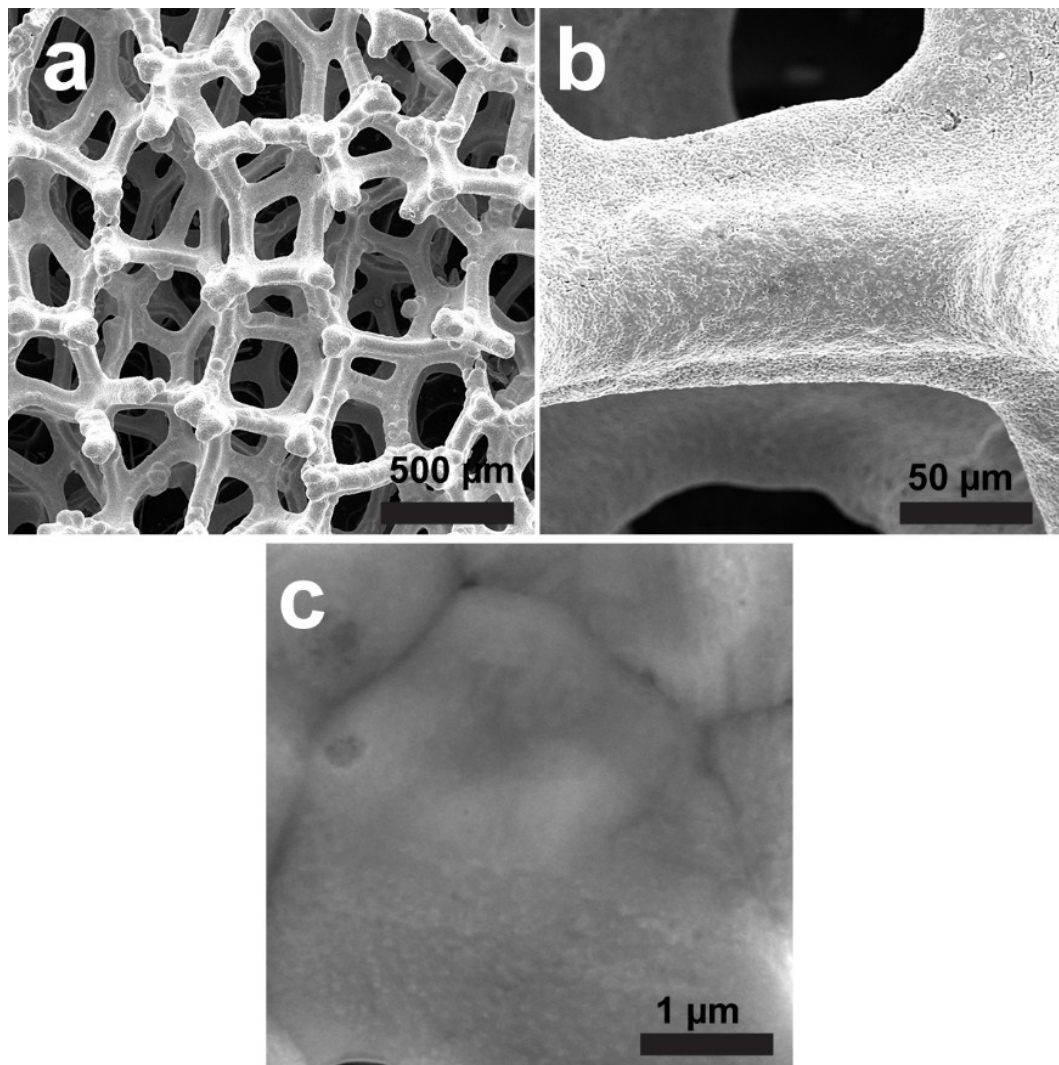


Figure S1. (a) and (b) Low-magnification SEM images of a bare Co foam (CF). (c) High-magnification SEM image of the surface of Co ligament.

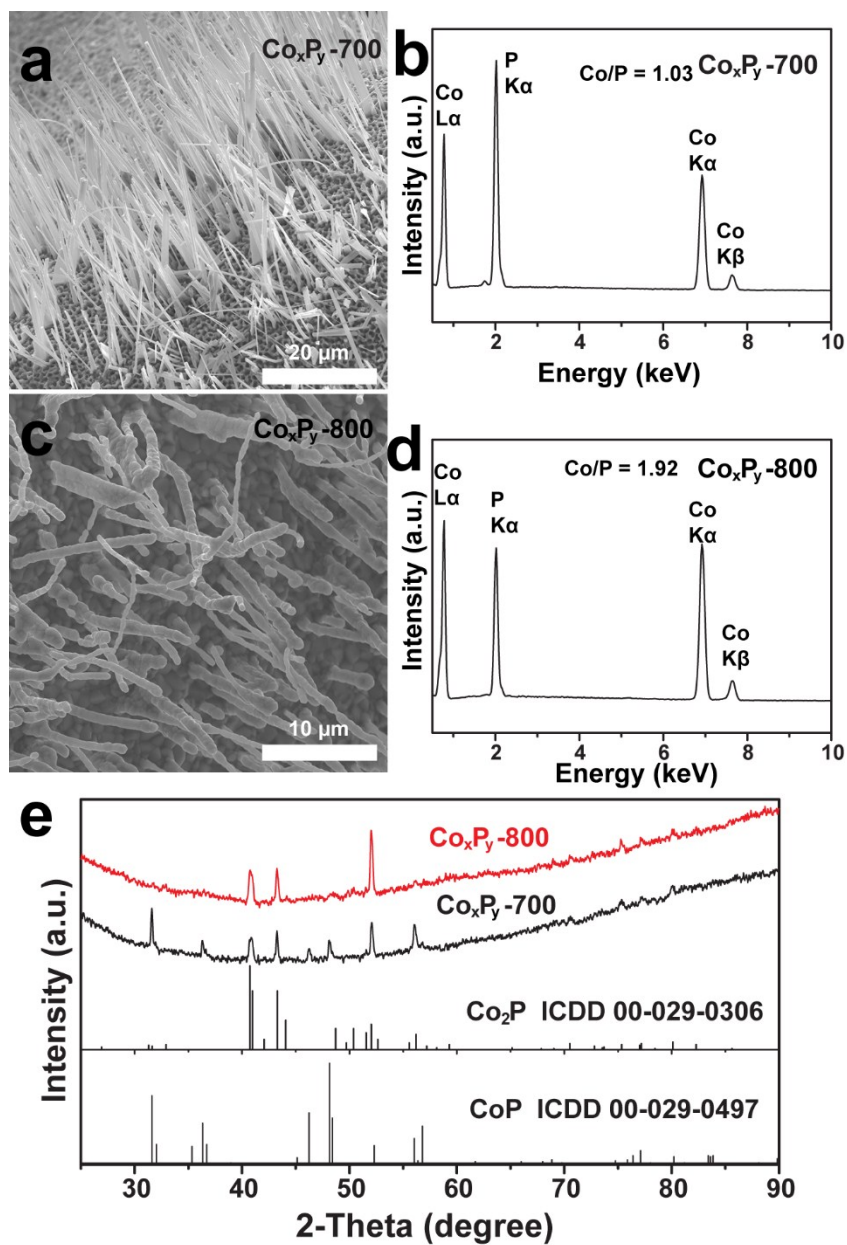


Figure S2. SEM image (a) and EDX spectrum (b) of Co_xP_y electrodes obtained at 700 °C (Co_xP_y -700). SEM image (c) and EDX spectrum (d) of Co_xP_y electrodes obtained at 800 °C (Co_xP_y -800). (e) XRD patterns of Co_xP_y -700 and Co_xP_y -800. The standard ICDD powder diffraction patterns of CoP (No. 00-029-0497) and Co_2P (No. 00-029-0306) are also given for reference.

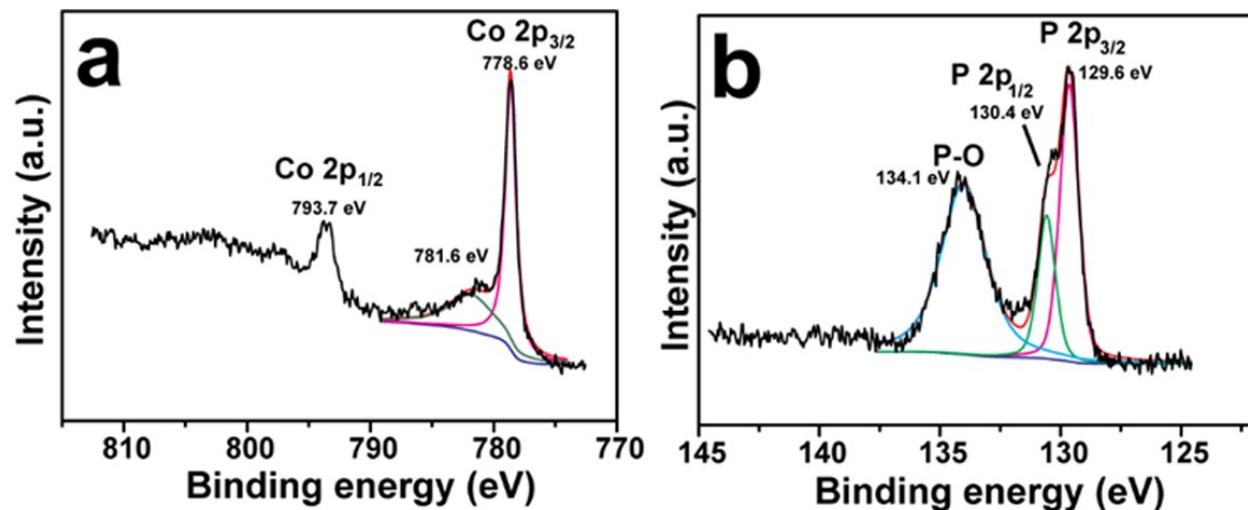


Figure S3. High-resolution XPS spectra of CoP NWs. (a) Co 2p peaks and (b) P 2p peaks.

In the typical Co 2p_{3/2} region, the sharp peak at 778.6 eV is assigned to Co 2p_{3/2} in the CoP component, consistent with the binding energy (BE) reported for CoP in the literature.^[1-5] The broad low-intensity peak at 781.6 eV corresponds to oxidized Co species that likely result from the slight surface oxidation. The presence of such an oxidation state is commonly observed in CoP nanostructures reported previously.^[3-5] In the P 2p region, the peaks at 129.6 and 130.4 eV are attributed to the P 2p_{3/2} and 2p_{1/2} of CoP, respectively, which are in good agreement with the BE in the reported CoP materials.^[1-5] The other peak at 134.1 eV corresponds to surface oxidized derivatives, which were reported in the literature.^[2-5] These assignments are well consistent with the BEs reported for CoP, demonstrating the good crystallinity of as-prepared CoP nanowires in this work.^[1-5]

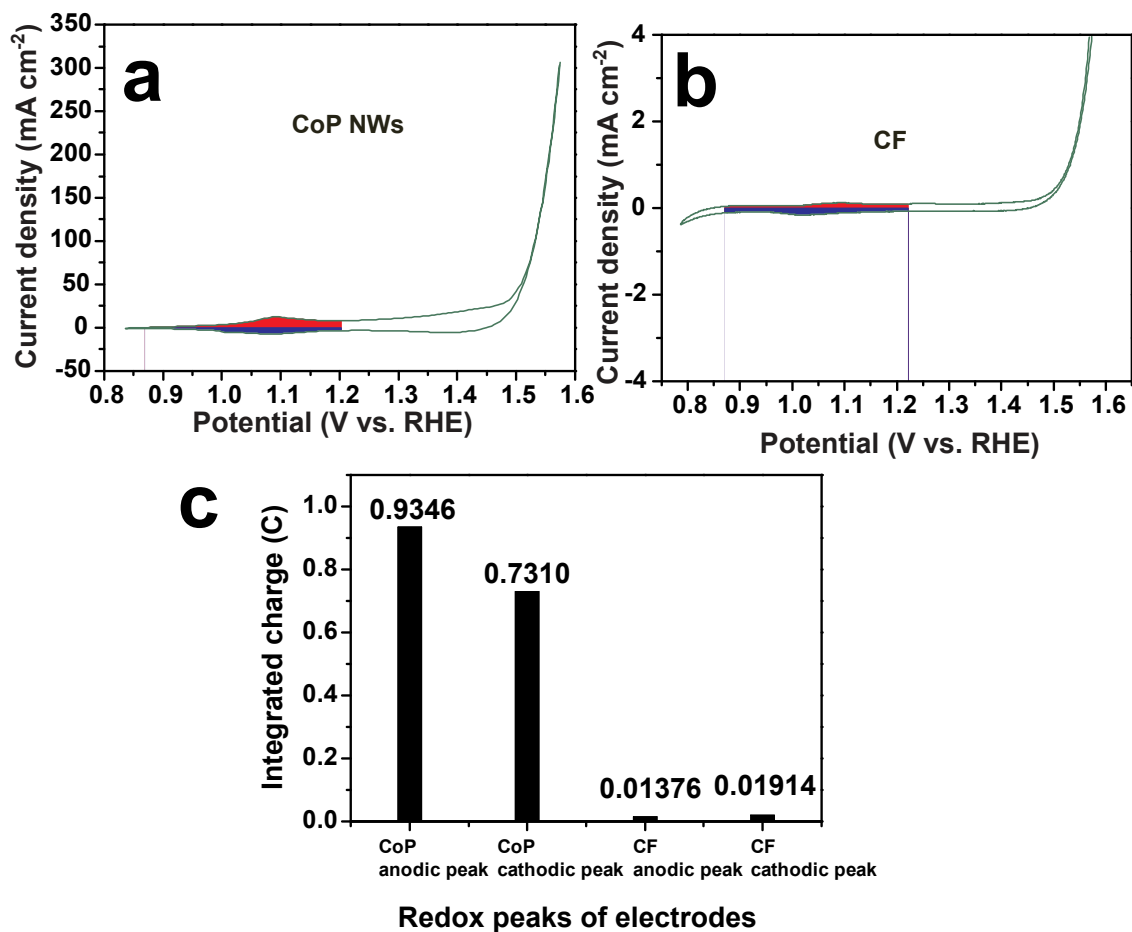


Figure S4. The steady-state cyclic voltammetric (CV) curves of the conditioned CoP NWs electrode (a) and bare Co foam (b) recorded at a rate of 2 mV s^{-1} . The shaded areas indicate the integration based on the oxidative (red) or reductive (blue) peak of the $\text{Co}^{2+} \leftrightarrow \text{Co}^{3+}$ redox pair. The integration potential window is $0.87 - 1.21 \text{ V vs. RHE}$. (c) Values of the integrated charges of the redox peaks for the conditioned CoP NWs and bare CF electrodes.

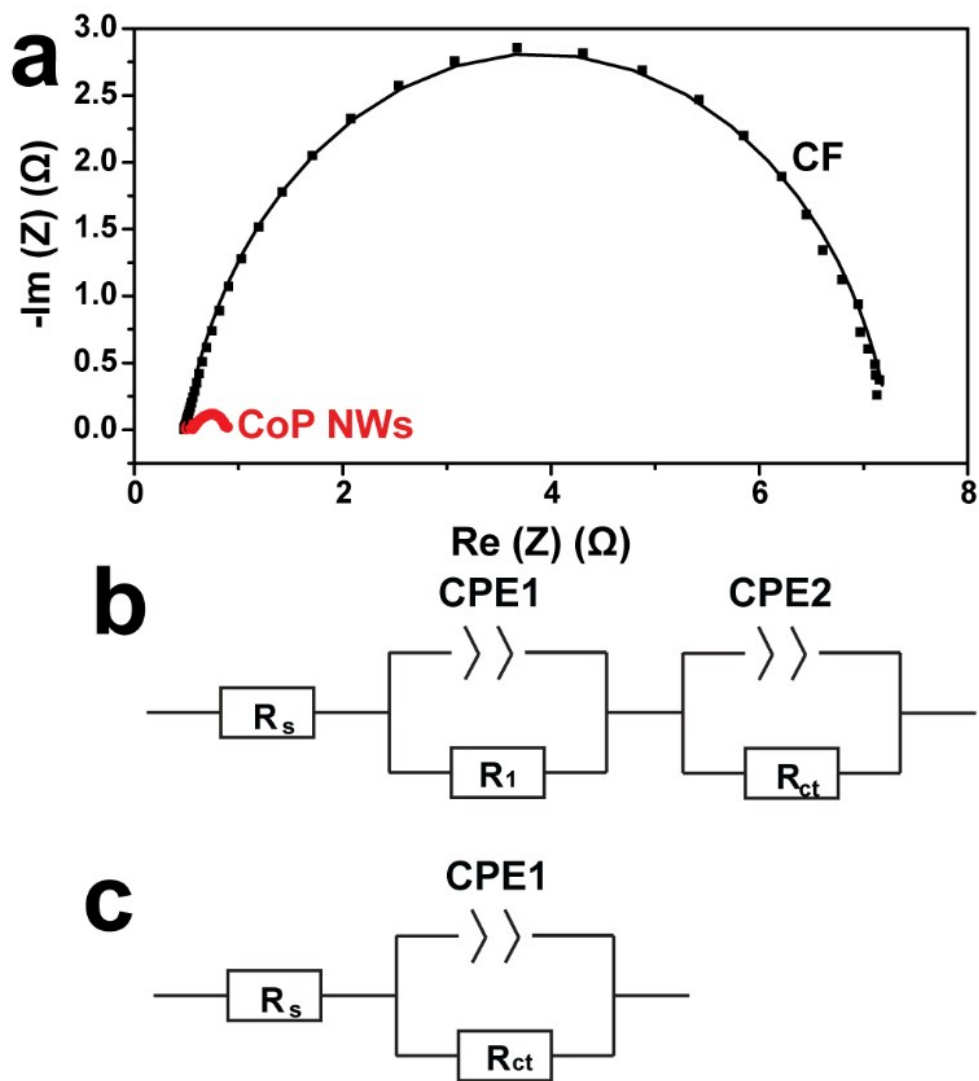


Figure S5. (a) Electrochemical impedance spectroscopy (EIS) Nyquist plots of the conditioned CoP NWs and bare CF electrodes recorded at 1.558 V vs. RHE in the frequency range of $2 \times 10^5 - 5 \times 10^{-3}$ Hz under the OER conditions. The data of conditioned CoP NWs and bare CF electrodes were fitted using the modified Randle equivalent circuit model shown in (b) and (c), respectively. R_s and R_{ct} represent the equivalent series resistance and charge transfer resistance.

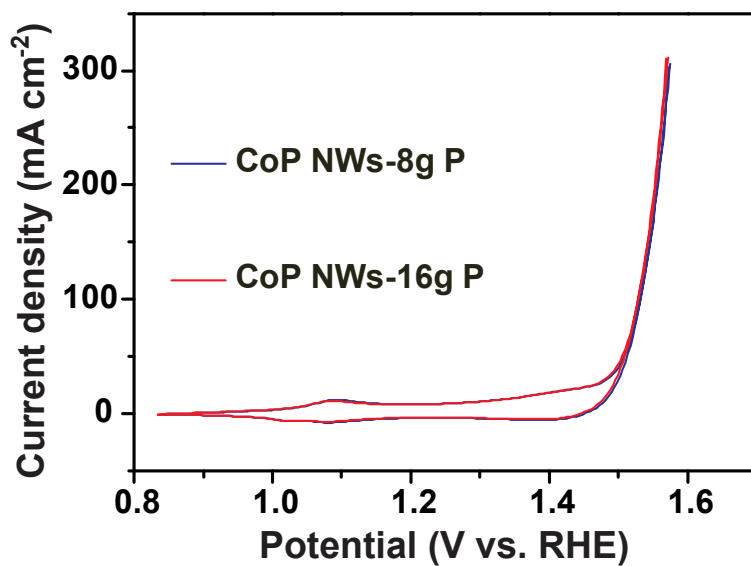


Figure S6. The steady-state cyclic voltammetric (CV) curves of the CoP NWs electrode obtained at 600 °C for 1 h in the presence of 8 and 16 g of red P. All experiments were conducted in 1.0 M KOH at room temperature.

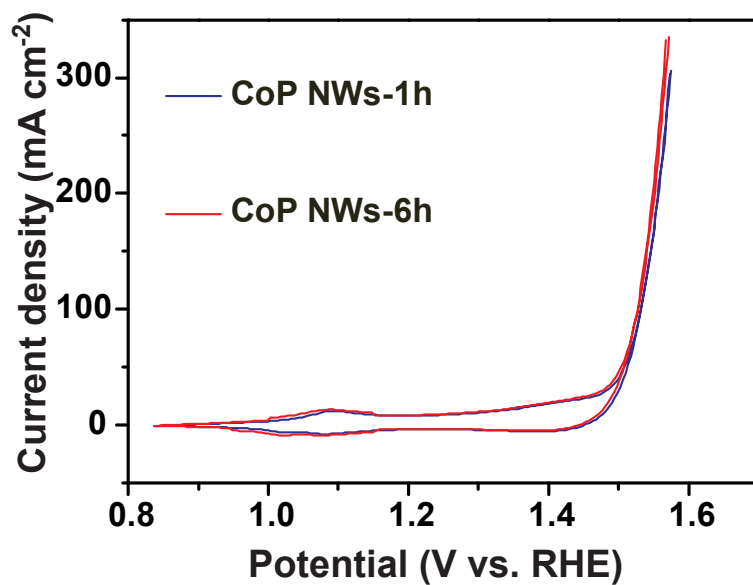


Figure S7. The steady-state cyclic voltammetric (CV) curves of the CoP NWs electrode obtained at 600 °C in the presence of 8 g of red P for 1 and 6 h. All experiments were conducted in 1.0 M KOH at room temperature.

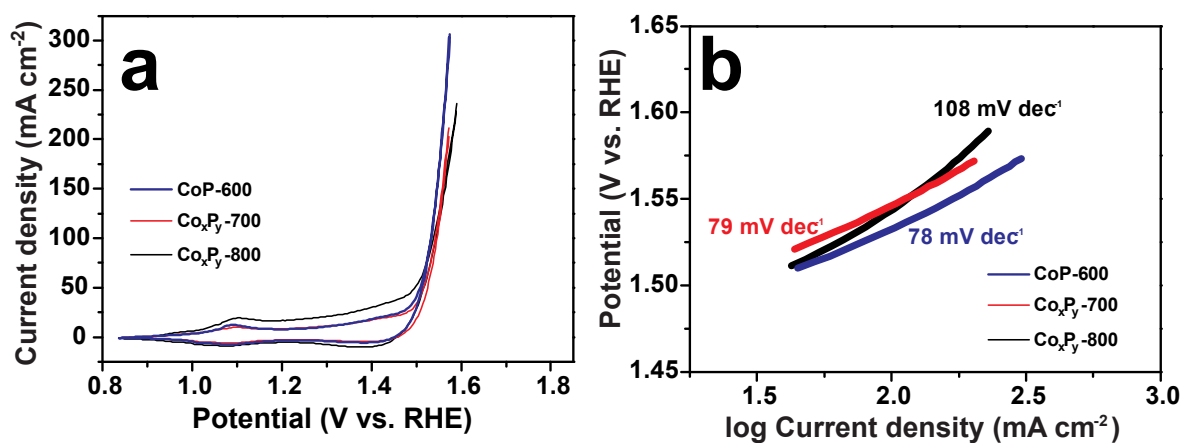


Figure S8. (a) The cyclic voltammetric (CV) curves of the cobalt phosphide electrodes synthesized at 600 (CoP-600), 700 (Co_xP_y-700) and 800 °C (Co_xP_y-800). (b) The Tafel plots of CoP-600, Co_xP_y-700 and Co_xP_y-800 derived from the reduction branches of their corresponding CV curves. All experiments were conducted in 1.0 M KOH at room temperature.

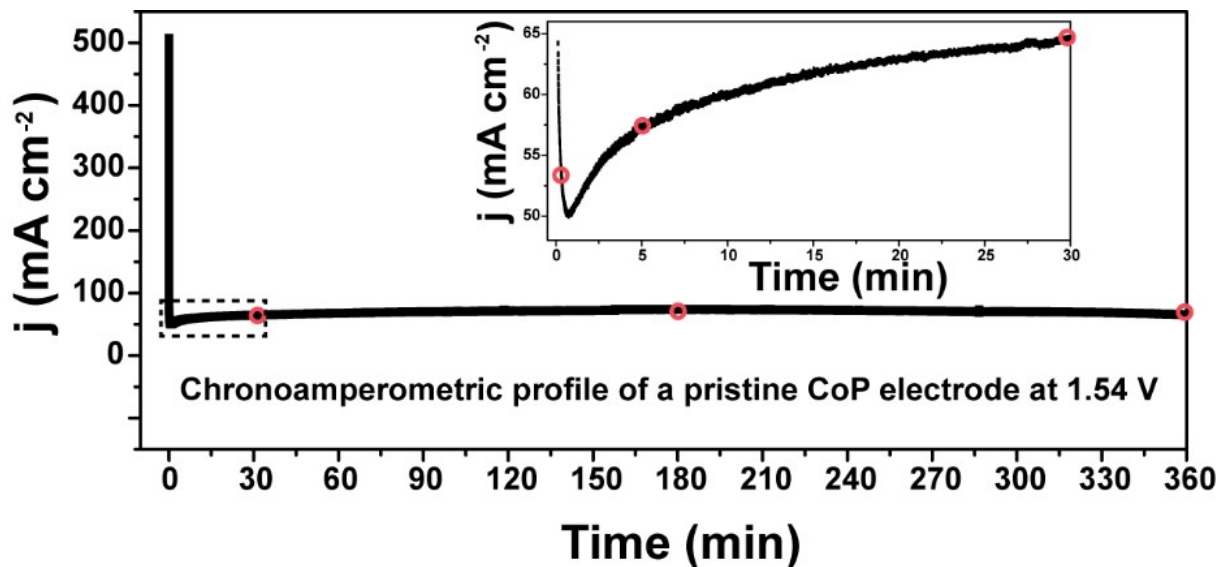


Figure S9. The chronoamperometric (CA) profile of a pristine CoP NWs electrode synthesized at 600 °C recorded at 1.54 V vs. RHE in 1.0 M KOH solution. Inset: zoomed view of the plot in the beginning 0.12 – 30 min. Five CoP NWs electrodes were examined comprehensively by SEM, TEM, Raman and XPS techniques, which are the ones after the CA test for only 20 s, 5 min, 30 min, 3 h and 6 h, respectively (the time points denoted by red open circles).

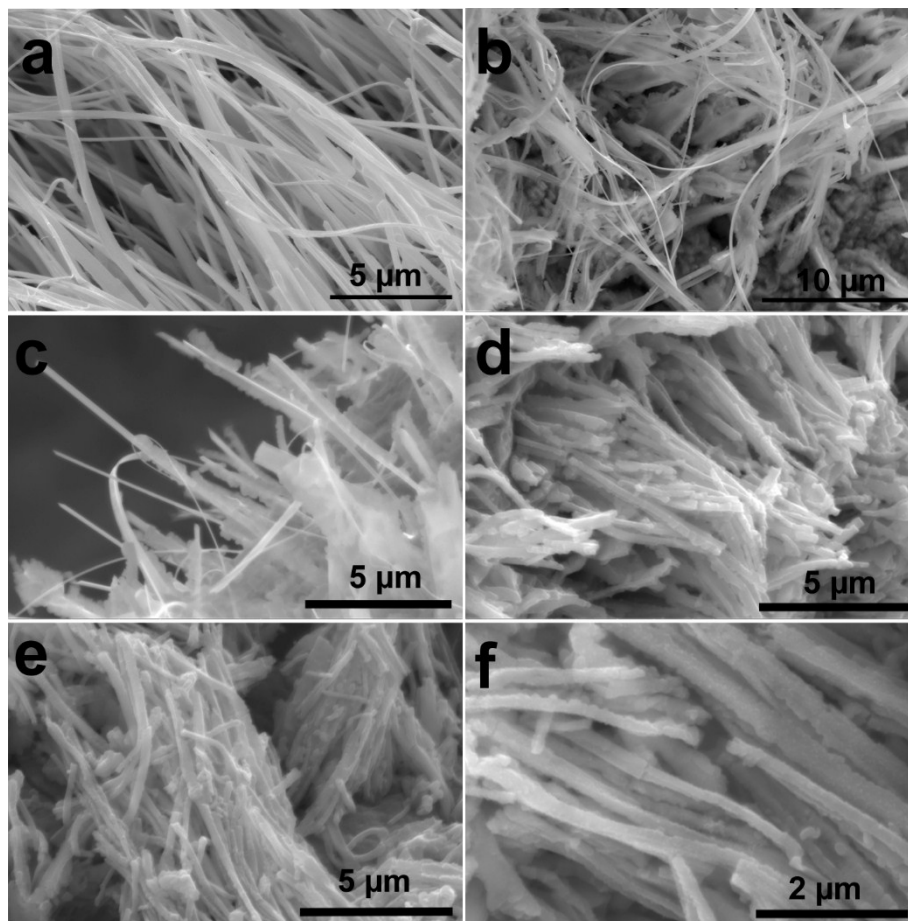


Figure S10. SEM images of the CoP NWs electrodes after the CA measurements at 1.54 V vs. RHE for 20 s (a), 5 min (b, c), 30 min (d), 3 h (e) and 6 h (f).

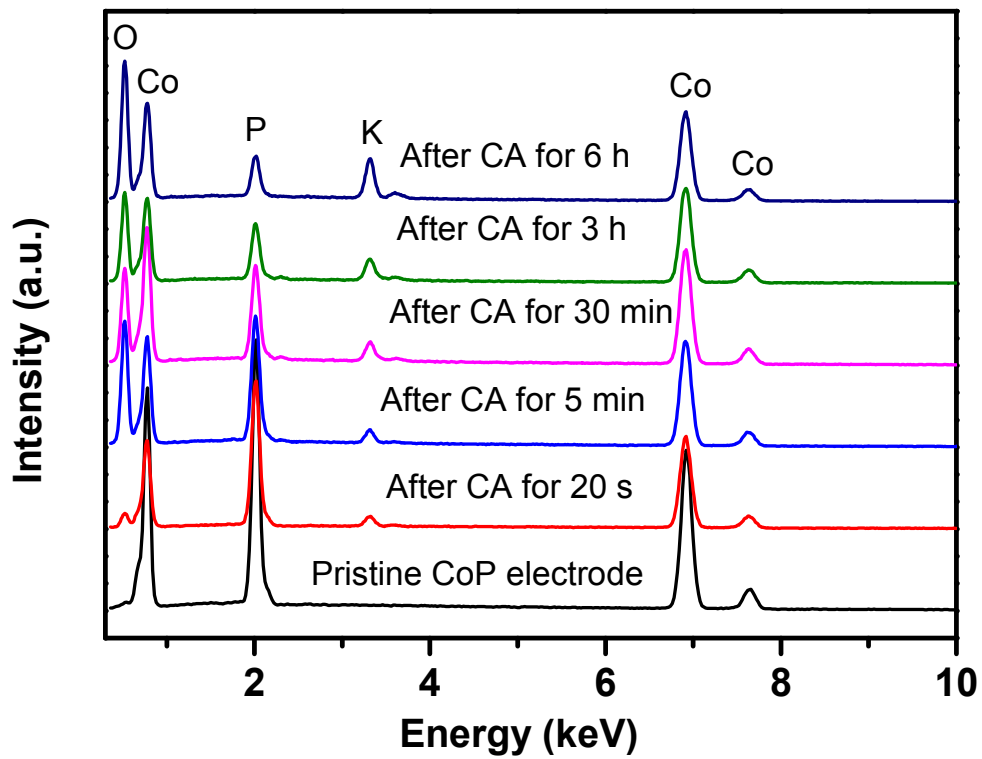


Figure S11. SEM-EDX spectra of the as-obtained CoP NWs electrode and those after the CA measurements at 1.54 V vs. RHE for a given period of time.

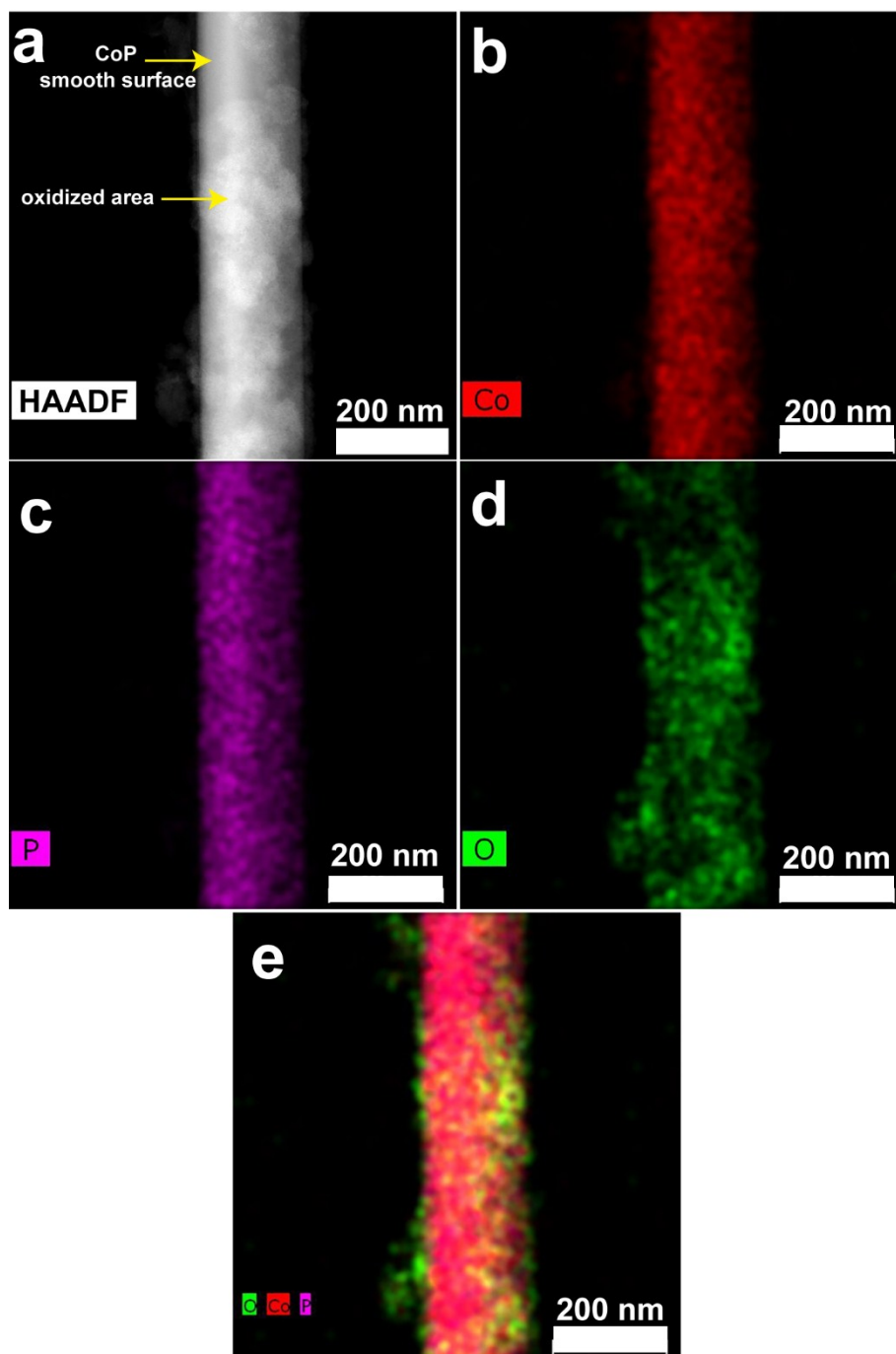


Figure S12. HAADF-STEM image (a) and elemental maps of Co (b), P (c), O (d) and their overlap (e) for a single NW after the CA measurement for 20 s at 1.54 V vs. RHE.

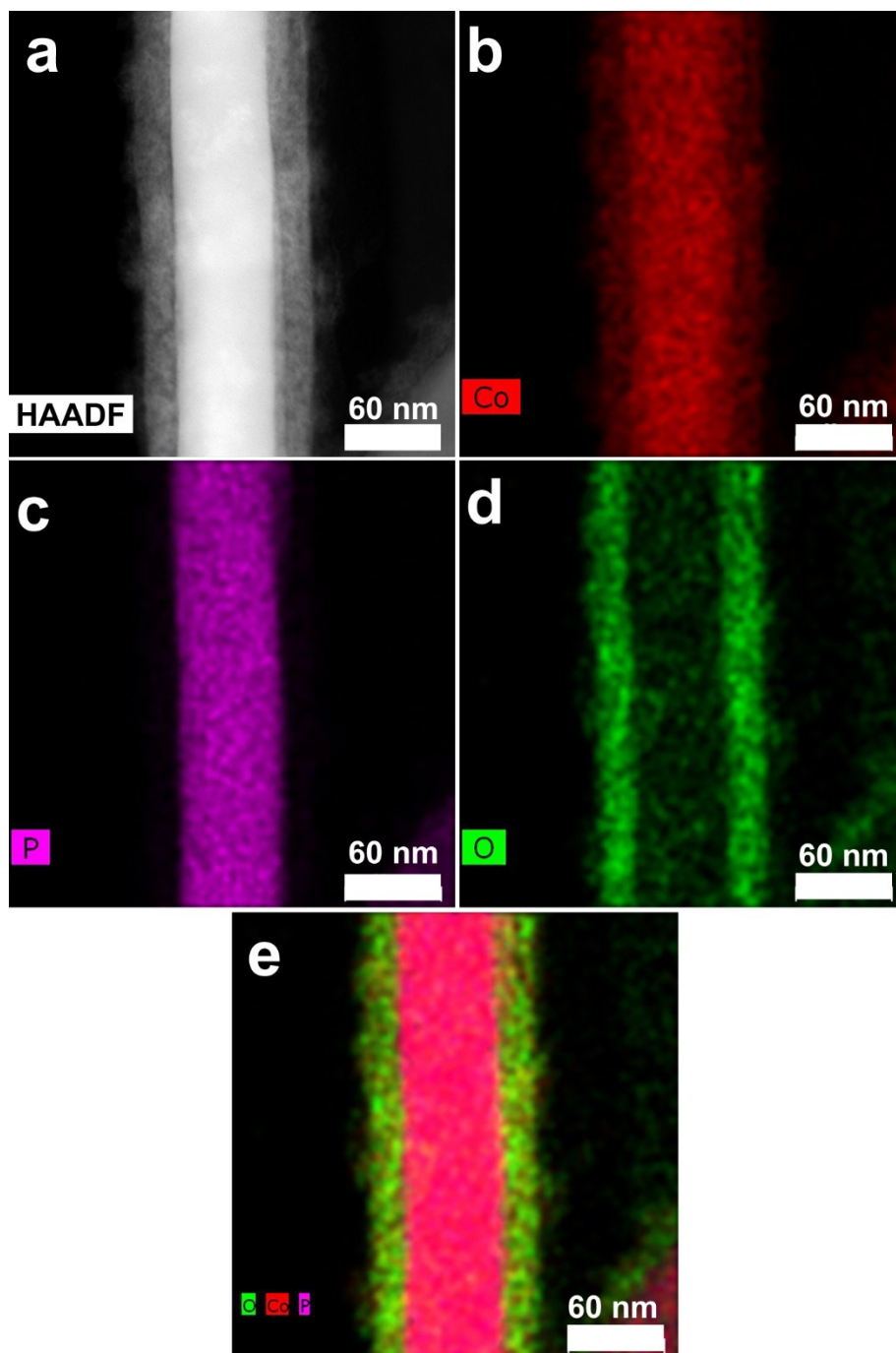


Figure S13. HAADF-STEM image (a) and elemental maps of Co (b), P (c), O (d) and their overlap (e) for a single NW after the CA measurement for 5 min at 1.54 V vs. RHE.

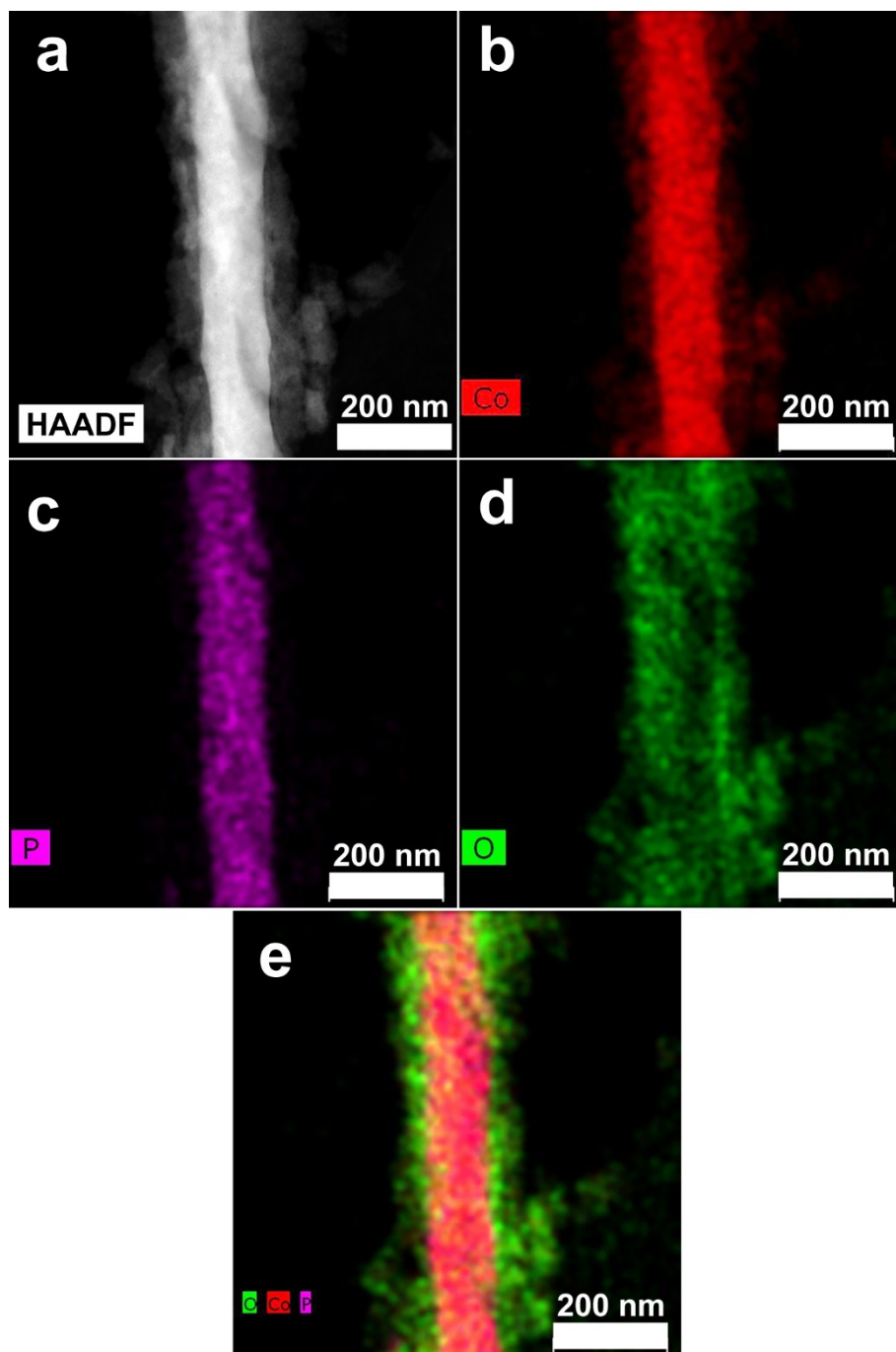


Figure S14. HAADF-STEM image (a) and elemental maps of Co (b), P (c), O (d) and their overlap (e) for a single NW after the CA measurement for 30 min at 1.54 V vs. RHE.

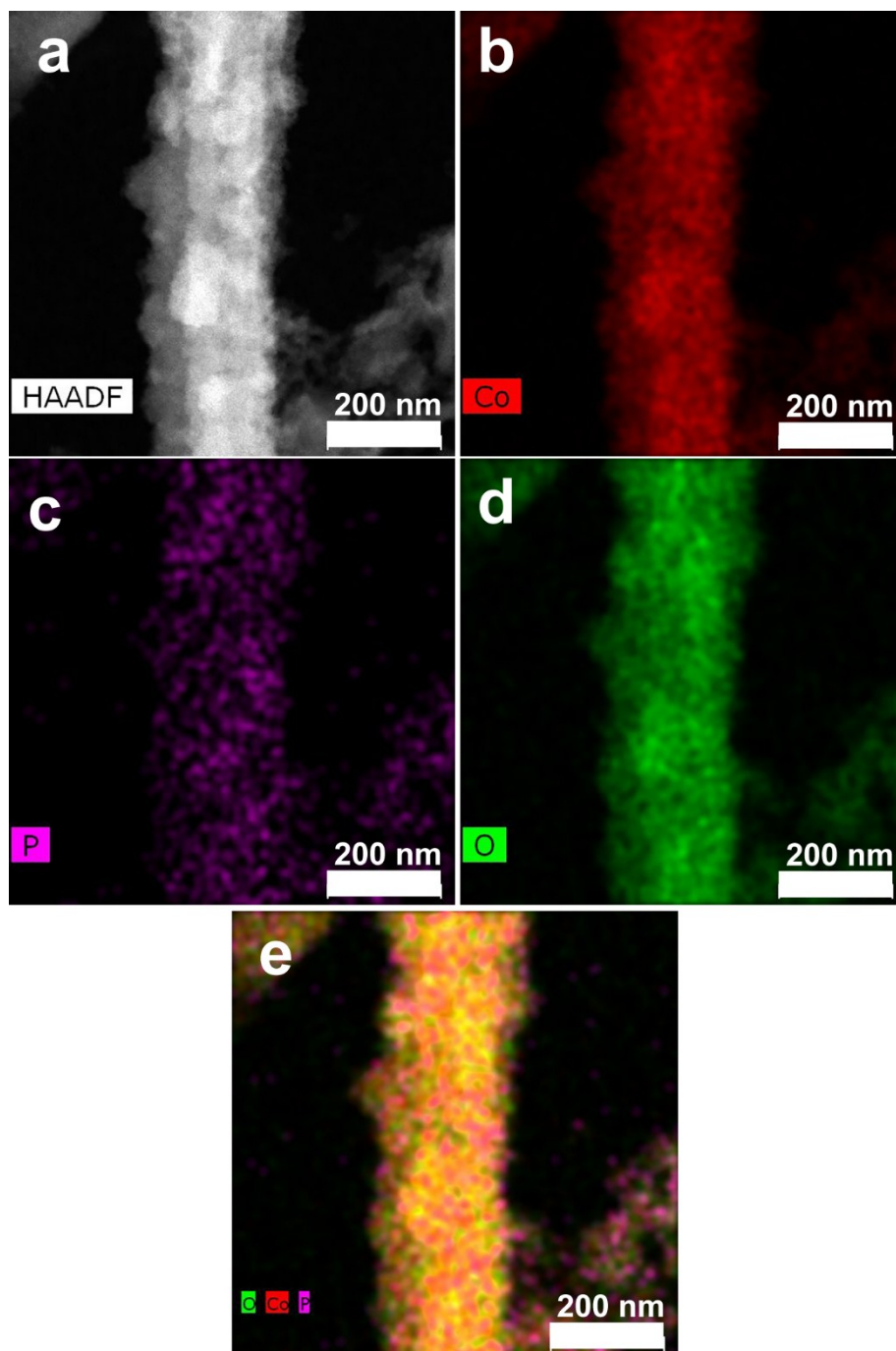


Figure S15. HAADF-STEM image (a) and elemental maps of Co (b), P (c), O (d) and their overlap (e) for a single NW after the CA measurement for 3 h at 1.54 V vs. RHE.

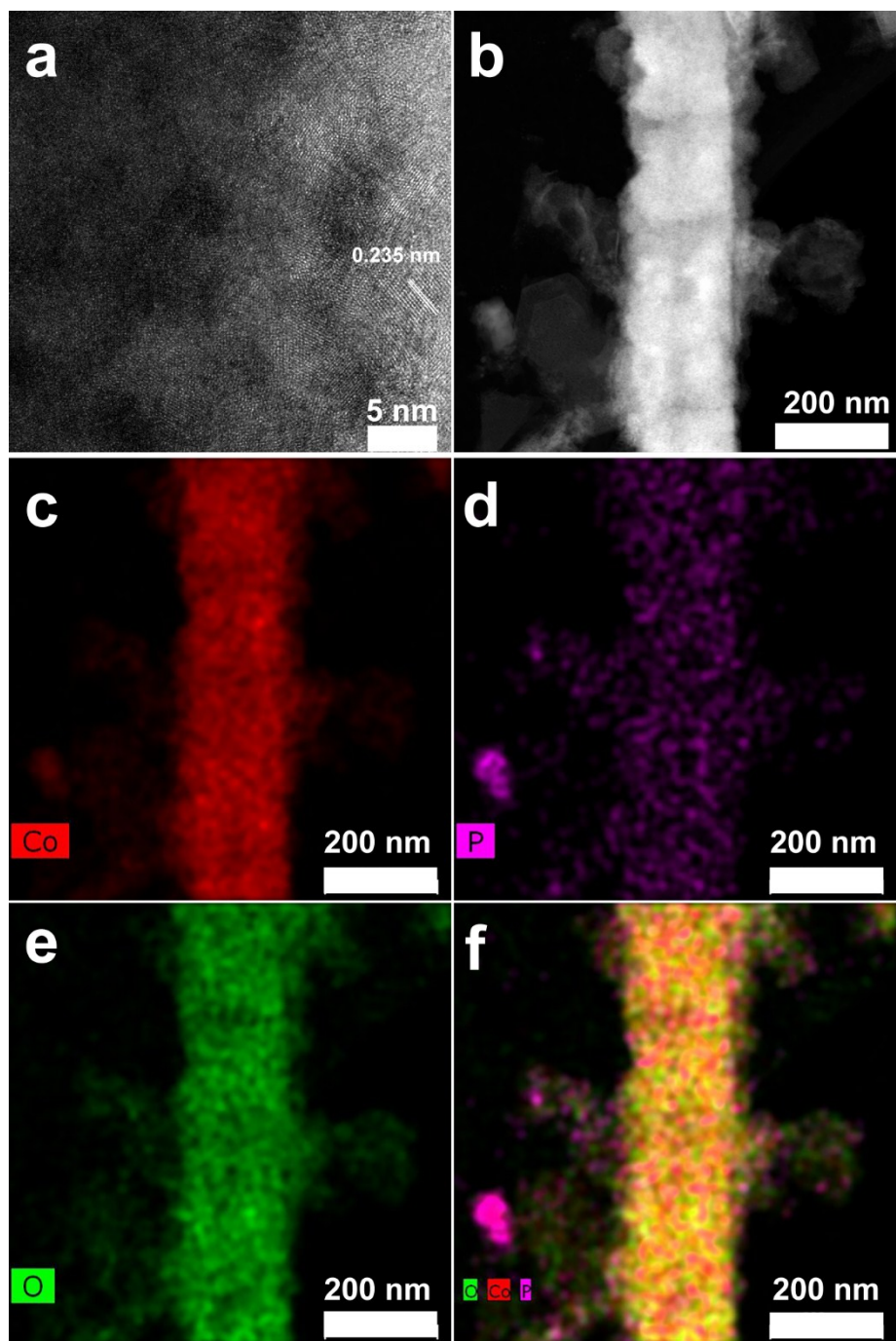


Figure S16. HRTEM image (a), HAADF-STEM image (b) and elemental maps of Co (c), P (d), O (e) and their overlap (f) for a single NW after the CA measurement for 6 h at 1.54 V vs. RHE.

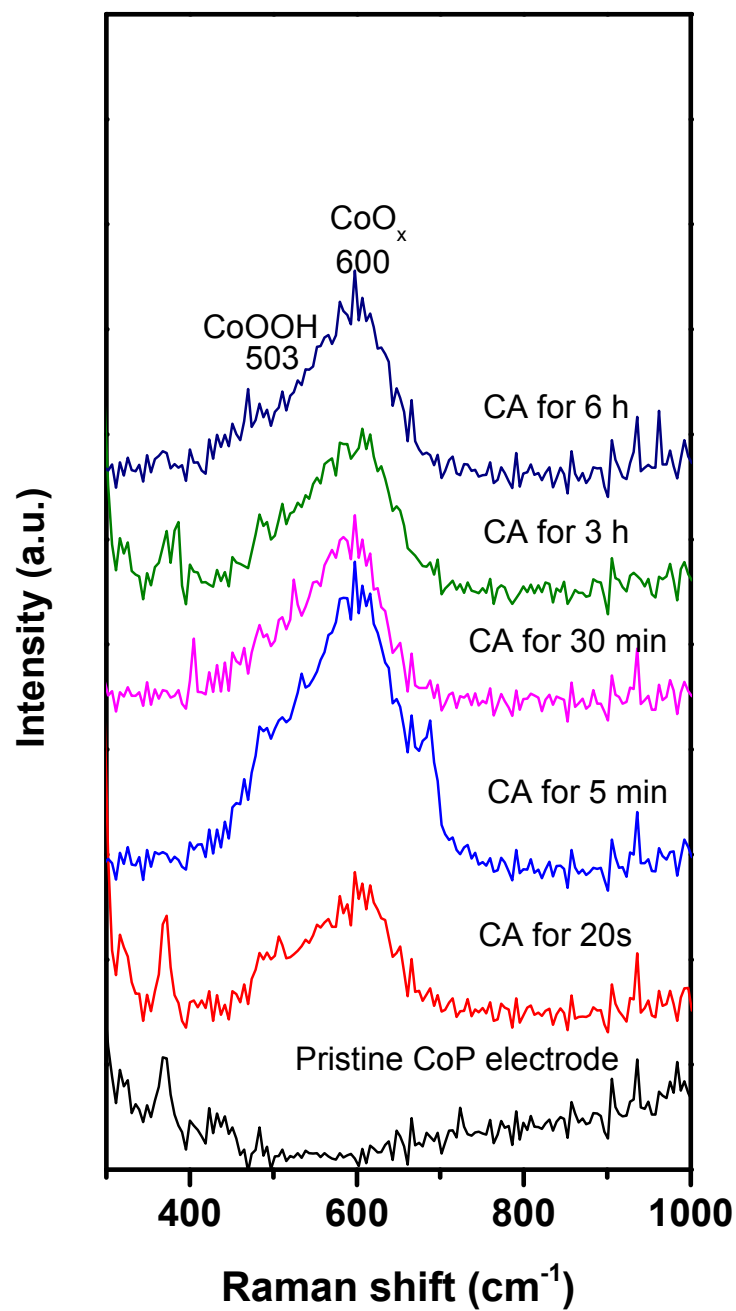


Figure S17. The Raman spectra of the pristine CoP electrode and those after the CA measurements at 1.545 V vs. RHE for the given time.

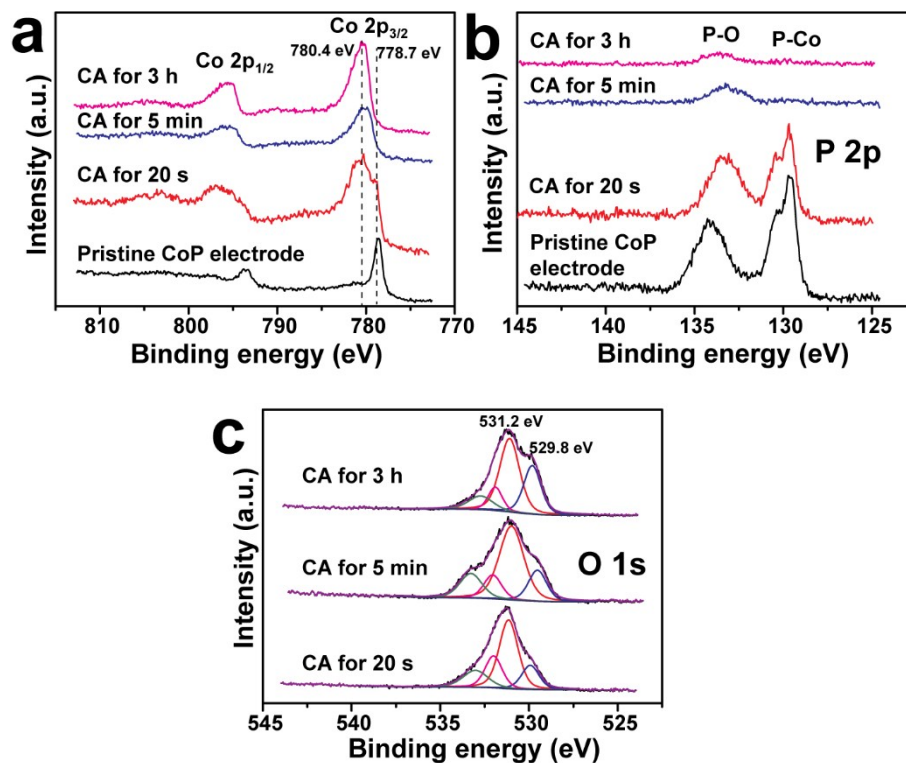


Figure S18. High-resolution XPS spectra of the pristine CoP NWs electrode and those after the CA measurements at 1.545 V vs. RHE for the given time. (a) Co 2p, (b) P 2p and (c) O 1s peaks.

The Co 2p_{3/2} peak at 778.7 eV corresponds to the Co species in CoP (*J. Am. Chem. Soc.*, 2014, 136, 7587-7590; *Nano Energy*, 2015, 15, 634-641; *Inorg. Chem.*, 2005, 44, 8988-8998). As the in-situ electrochemical oxidation/dephosphorization proceeds, the intensities of P 2p peaks attributed to CoP significantly decrease, and the Co 2p_{3/2} peak at 780.4 eV and deconvoluted O 1s peaks at 531.2 and 529.8 eV become prominent, which can be assigned to the formed CoOOH (J. Ryu, N. Jung, J. H. Jang, H.-J. Kim and S. J. Yoo, *ACS Catal.*, **2015**, 5, 4066-4074; M. S. Burke, M. G. Kast, L. Trotochaud, A. M. Smith and S. W. Boettcher, *J. Am. Chem. Soc.*, **2015**, 137, 3638-3648;

J. Yang, H. Liu, W. N. Martens and R. L. Frost, *J. Phys. Chem. C*, **2010**, 114, 111-119). This indicates that CoOOH starts to appear in the CA-20 s electrode and the CoP NWs are in-situ converted to CoOOH progressively, while P is leaching out as the electrolysis proceeds.

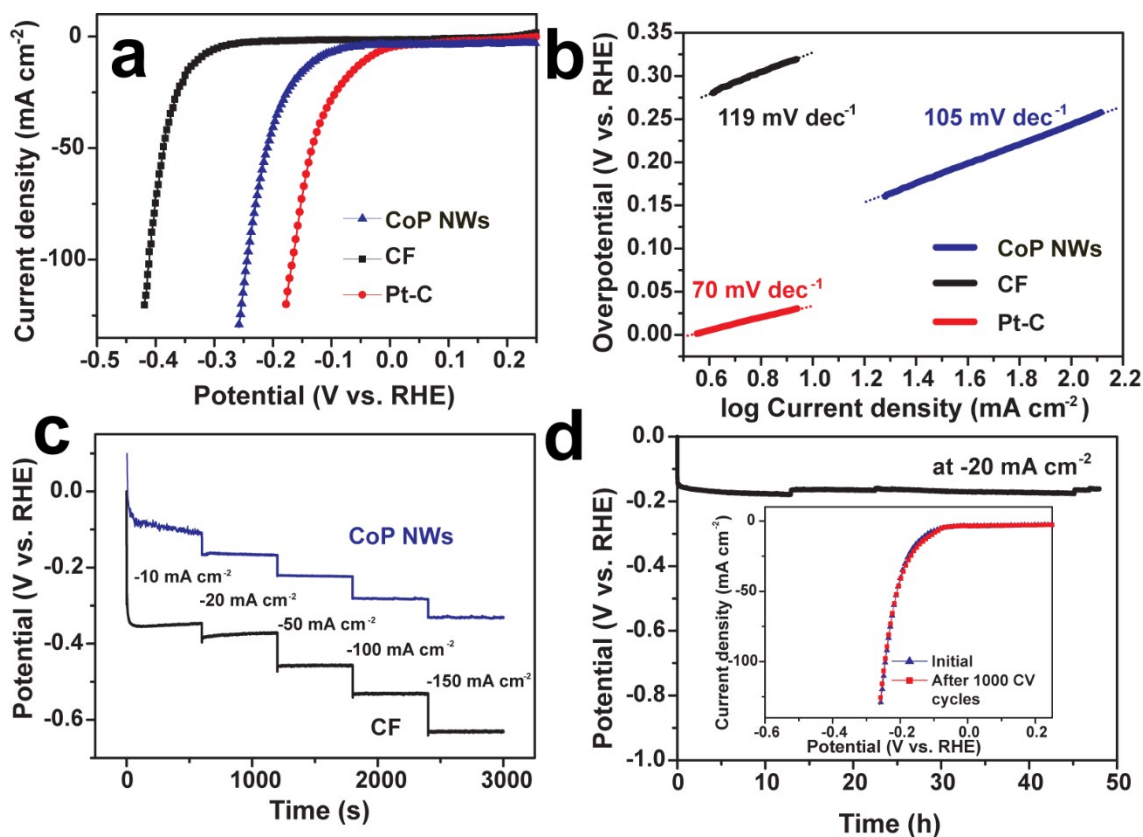


Figure S19. Electrocatalytic performance of the electrodes for the HER measured in H₂-saturated 1.0 M KOH. (a) Polarization curves of CoP NWs synthesized at 600 °C, bare CF and Pt-C catalysts deposited on CF. (b) The corresponding Tafel plots. (c) Multi-step chronopotentiometric (CP) curves of CoP NWs and CF at varying current densities without iR-correction. (d) The CP curve

of CoP NWs recorded at a current density of -20 mA cm^{-2} . Inset is the polarization curves of the CoP NWs electrode before and after 1000 continuous CV cycles in the range of $-0.22 - 0.2 \text{ V}$ at a scan rate of 50 mV s^{-1} .

The monolithic CoP NWs foam was also used as an integrated electrode to catalyze the HER in H_2 -saturated 1.0 M KOH in a three-electrode configuration. **Figure S19** shows the polarization curves of CoP NWs, CF and Pt-C catalyst supported on CF measured under the same conditions. As the state-of-the-art electrocatalyst for HER, Pt-C exhibits the highest electrocatalytic activity, delivering a current density of -10 mA cm^{-2} at -39 mV . The CoP NWs electrode only requires overpotentials of 124 mV (η_{10}), 163 mV (η_{20}) and 244 mV (η_{100}) to deliver current densities of -10 , -20 and -100 mA cm^{-2} respectively, outperforming those of many recently-reported non-precious HER catalysts tested under the similar conditions (**Table S2**). In contrast, the bare CF shows a small current density of merely -5.7 mA cm^{-2} even at a high overpotential of 300 mV . The Tafel slope of CoP NWs is 105 mV dec^{-1} , which is much smaller than that of CF (119 mV dec^{-1}) and favorably comparable to those of many recently-reported non-precious HER catalysts (**Table S2**). The Tafel slope falls within the range of $40-120 \text{ mV dec}^{-1}$, suggesting that the HER taking place on the CoP surface in the basic solution would follow a Volmer–Heyrovsky mechanism, and that the rate of the discharge step would be consistent with that of the desorption step.^[6, 7] **Figure S19c** illustrates multi-step chronopotentiometric (CP) curves of CoP NWs and CF recorded under varying current densities from -10 to -150 mA cm^{-2} without iR-correction. Upon increasing the cathodic current density, the potential of CoP NWs grows and gets stabilized rapidly, suggesting its excellent mass transfer characteristic and mechanical stability. The overpotential of CoP NWs is substantially lower than that of bare CF at any given cathodic current, demonstrating its superior rate capability. The CoP NWs electrode only needs a small overpotential of 331 mV (non iR-corrected) to deliver a

high current density of -150 mA cm^{-2} . The CoP NWs electrode shows remarkable long-term durability under a stable potential of ca. -0.164 V to afford a current density of -20 mA cm^{-2} for 48 h. Even after 1000 continuous CV cycles scanned from -0.22 to 0.2 V , the CoP NWs electrode still displays a similar polarization to initial one with negligible degradation, indicative of remarkable stability. The outstanding HER electrocatalytic activity of the CoP NWs electrode is likely attributed to the dense thin CoP nanowires with high aspect ratio, which not only maximizes the number of exposed active sites, but also facilitates the diffusion of electrolyte and the release of generated gas bubbles.^[5]

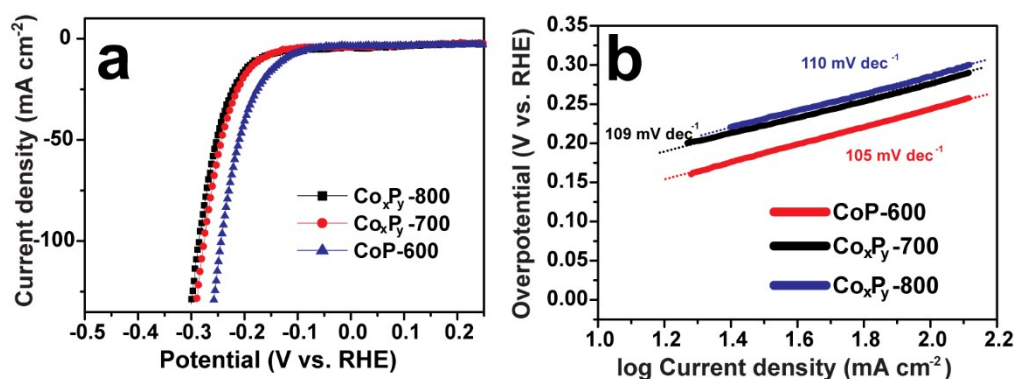


Figure S20. (a) The polarization curves and Tafel plots of the CoP electrodes synthesized at 600 (CoP-600), 700 (Co_xP_y-700) and 800 °C (Co_xP_y-800).

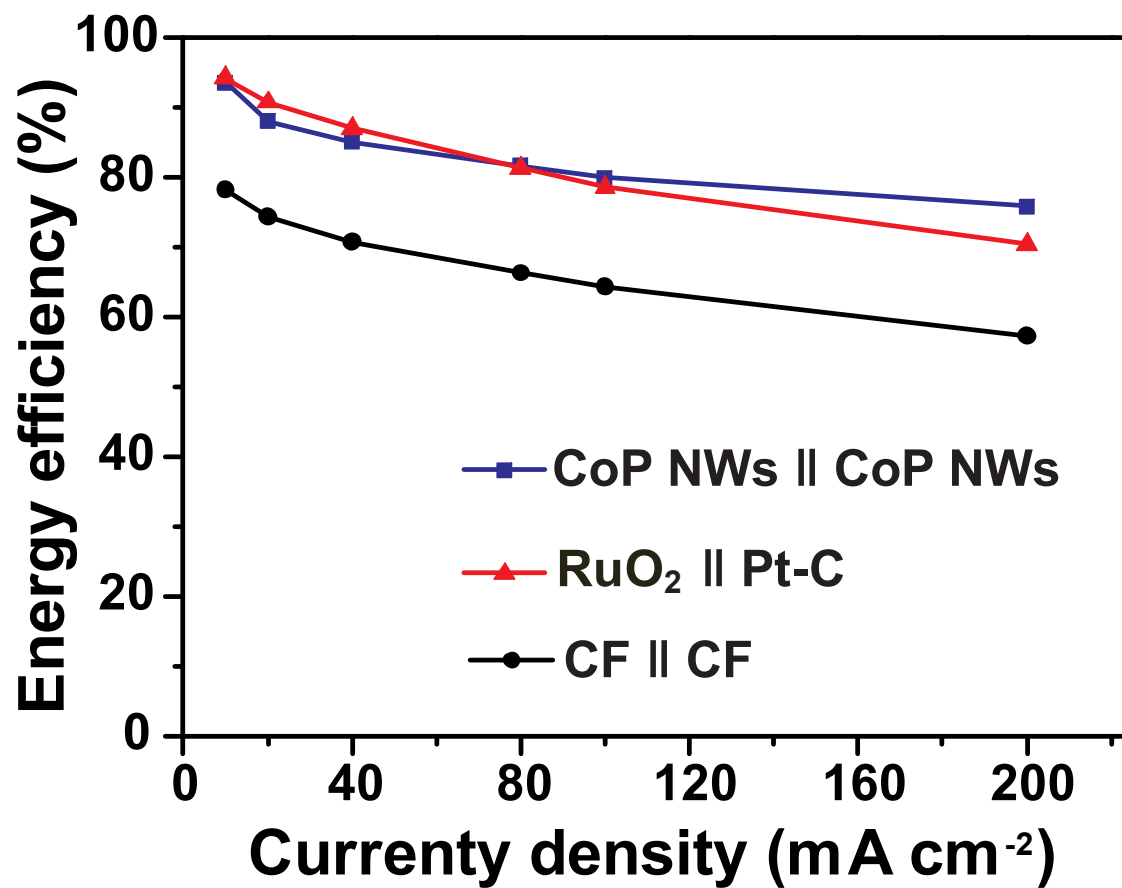


Figure S21. Energy efficiency of the CoP NWs, RuO₂||Pt-C and CF electrolyzers for overall water splitting in 1.0 M KOH solution as a function of current density.

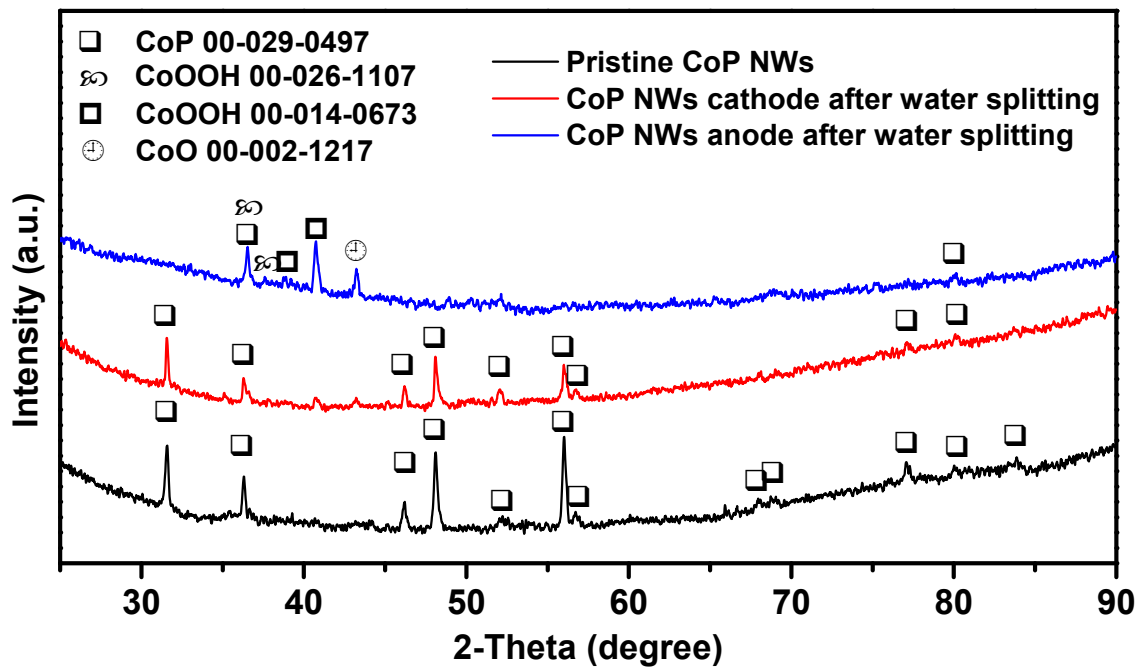


Figure S22. XRD patterns of the pristine CoP NWs, CoP NWs cathode and in-situ oxidized CoP NWs anode after overall water splitting in 1.0 M KOH at 20 mA cm⁻² for 1000 h.

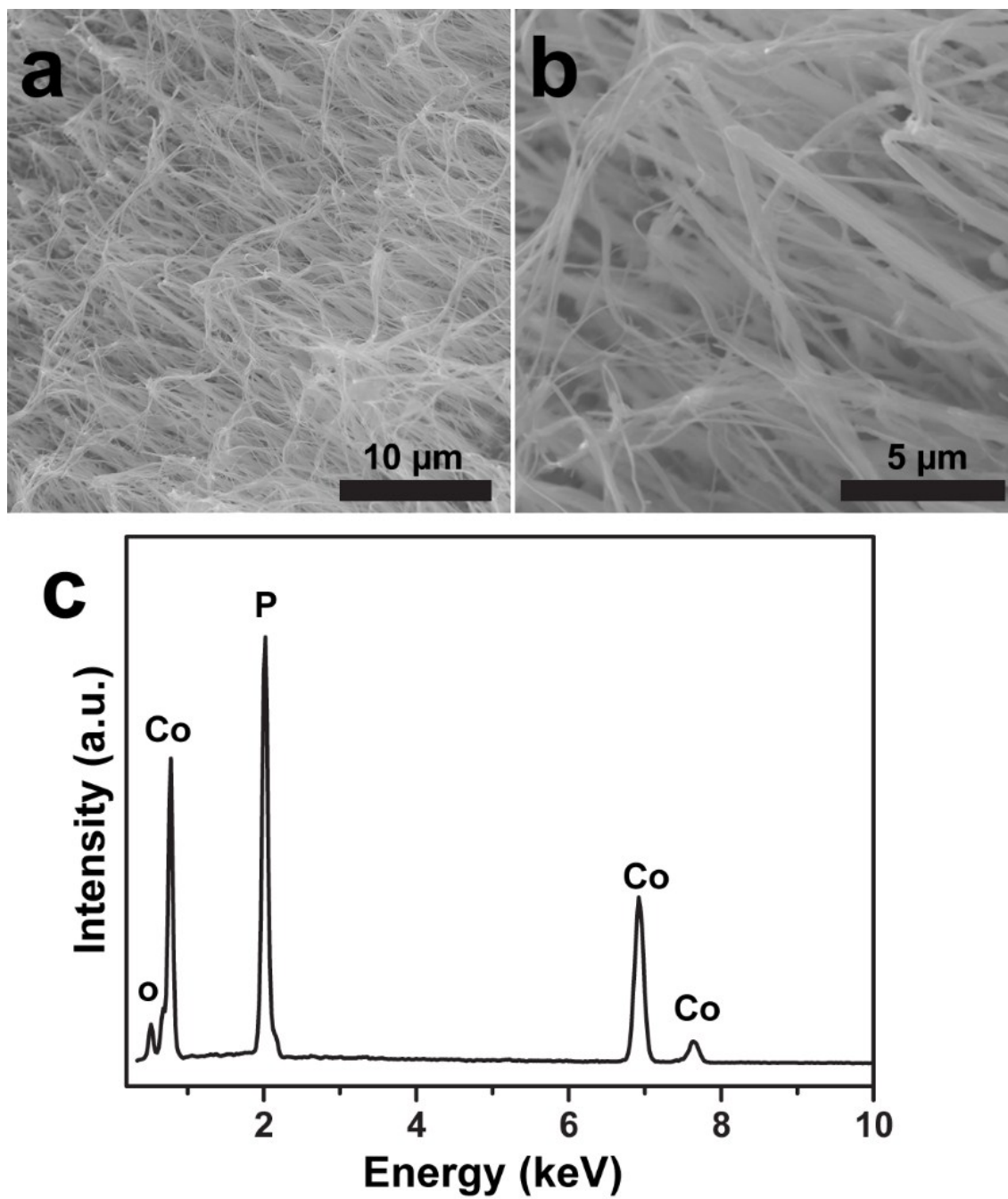


Figure S23. SEM images (a, b) and EDX spectrum (c) of the CoP NWs cathode after overall water splitting in 1.0 M KOH at 20 mA cm⁻² for 1000 h.

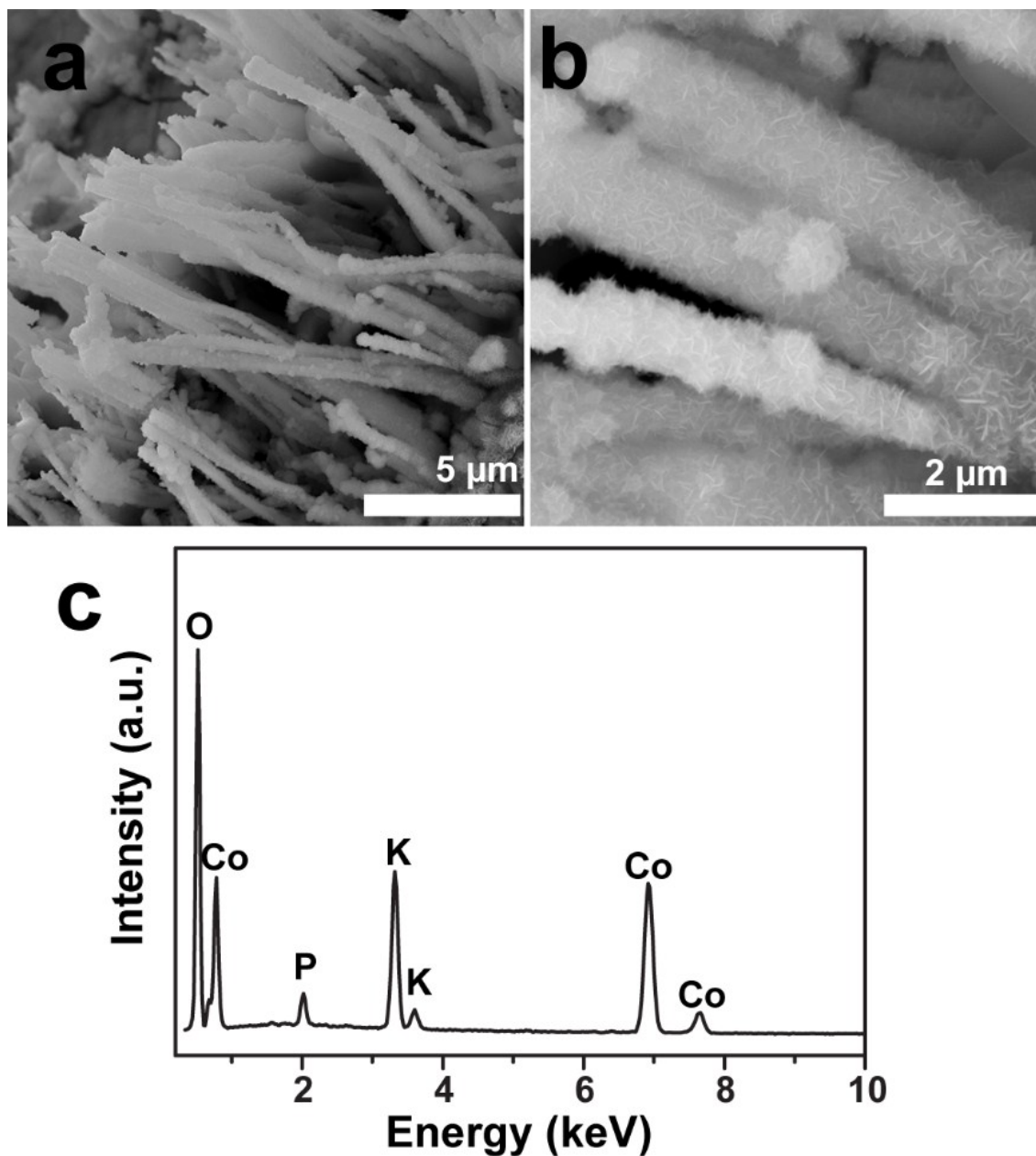


Figure S24. SEM images (a, b) and EDX spectrum (c) of the in-situ oxidized CoP NWs anode after overall water splitting in 1.0 M KOH at 20 mA cm⁻² for 1000 h.

Table S1 Comparison of the electrocatalytic performance of the in-situ oxidized CoP NWs electrode for the OER with that of reported non-precious metal electrocatalysts tested under similar conditions.

Electrocatalyst	Electrolyte	η_{10} (mV vs. RHE) ^a	η_{20} (mV vs. RHE) ^b	η_{100} (mV vs. RHE) ^c	Tafel slope (mV dec ⁻¹)	Reference
In-situ electrochemically oxidized CoP NWs	1.0 M KOH	248	261	300	78	This work
Co-P film	1.0 M KOH	345	370	413	47	<i>Angew. Chem. Int. Ed.</i> 2015 , 54, 6251.
Cobalt phosphide/phosphate film	1.0 M KOH	310	320		165	<i>Adv. Mater.</i> 2015 , 27, 3175.
CoP nanoparticle	0.1 M KOH	360	380		83	<i>ACS Catal.</i> 2015 , 5, 4066.
Co ₂ P foil	1.0 M KOH	360	380		65	<i>Energy Environ. Sci.</i> , 2016 , 9, 2257.
(Co _{0.52} Fe _{0.48}) ₂ P foil	1.0 M KOH	270	290		30	
Co ₂ P	1.0 M KOH	370	390		128	<i>J. Am. Chem. Soc.</i> 2016 , 138, 4006.
CoP and Co ₂ P in N-doped carbon	1.0 M KOH	319	350	410	88	<i>Chem. Mater.</i> 2015 , 27, 7636.
Co-Ni-P NWs	1.0 M KOH	300	320	360	65	<i>J. Power Source</i> , 2016, 330, 156.
Ni ₅ P ₄ nanosheets on Ni foil	1.0 M KOH	290	310			<i>Angew. Chem. Int. Ed.</i> 2015 , 54, 12361.
Ni ₂ P	1.0 M KOH	290	300		59	<i>Energy Environ. Sci.</i> , 2015 , 8, 2347.
NiFe LDH	1.0 M NaOH	250	270	470		<i>Science</i> 2014 , 345, 1593.
Ni(OH) ₂ nanocages	1.0 M KOH	> 470			182	<i>Adv. Energy Mater.</i> 2015 , 5, 1401880.
Ni ₂ Co(OH) _x nanocages	1.0 M KOH	> 470			135	
NiCo _{2.7} (OH) _x nanocages	1.0 M KOH	350	380		109	
Co(OH) ₂ nanocages	1.0 M KOH	390	420			
NiCo LDH	1.0 M KOH	474	500		66	<i>Nano Lett.</i> 2015 , 15, 1421.
CoSe ₂ sheets	1.0 M KOH	340	370		64	<i>Angew. Chem. Int. Ed.</i> 2015 , 54, 12004.
CoSe ₂ nanosheets	0.1 M KOH	320	370		84	<i>J. Am. Chem. Soc.</i> 2014 , 136, 15670.
Ni ₃ S ₂ /Ni foam	1.0 M KOH	320	330		159.3	<i>Energy Environ. Sci.</i> 2013 , 6, 2921.

MoO ₂	1.0 M KOH	260	280		116	<i>Adv. Mater.</i> 2016 , 28, 3785.
V/Ni foam	1.0 M KOH	292	320	350	125	<i>Nanoscale</i> 2016 , 8, 10731.

^a The overpotential required to deliver 10 mA cm⁻². ^b The overpotential required to deliver 20 mA cm⁻². ^c The overpotential required to deliver 100 mA cm⁻². Note that the values of single-crystalline CoP NWs in this work were obtained from the reduction branch of its CV in **Figure 3a**, while those reported values in the references were obtained from their LSV polarization curves in the literature.

Table S2. Comparison of the electrocatalytic performance of the CoP NWs electrode for the HER with that of non-precious metal electrocatalysts reported in the literature. Unless stated otherwise, the HER tests were made in 1.0 M KOH solution.

Electrocatalyst	η_{10} (mV vs. RHE) ^a	η_{20} (mV vs. RHE) ^b	η_{100} (mV vs. RHE) ^c	Tafel slope (mV dec ⁻¹)	Reference
Single-crystalline CoP NWs	124	163	244	105	This work
EG/Co _{0.85} Se/NiFe-LDH	260	ca. 330	-	160	<i>Energy Environ. Sci.</i> , 2016 , 9, 478.
EG/Co _{0.85} Se	325	440	-	223	<i>Energy Environ. Sci.</i> , 2016 , 9, 478.
CoSe ₂ /carbon cloth	190	300	-	85	<i>Adv. Mater.</i> , 2016 , 28, 7527.
CoSe ₂ nanocrystals	450	600	-	126	<i>ACS Appl. Mater. Interfaces</i> , 2016 , 8, 5327.
Co-P film on Cu foil	94	115	158	42	<i>Angew. Chem. Int. Ed.</i> 2015 , 54, 6251
Polycrystalline CoP NWs on carbon cloth	209	250	> 500	129	<i>J. Am. Chem. Soc.</i> 2014 , 136, 7587
Porous Co-P film	380	410	> 450		<i>Adv. Mater.</i> 2015 , 27, 3175
Co-embedded nitrogen-rich CNTs	370	450		69	<i>Angew. Chem. Int. Ed.</i> 2014 , 53, 4372
Ni ₂ P nanoparticles	170	205			<i>J. Am. Chem. Soc.</i> 2013 , 135, 9267
Ni ₂ P nanoparticles	220	250		100	<i>Phys. Chem. Chem. Phys.</i> 2014 , 16, 5917
MoS _{2+x} on Ni foam	210	220	335	84	<i>Angew. Chem. Int. Ed.</i> 2015 , 54, 664
Ni ₅ P ₄ nanosheets on Ni foil	150	170		53	<i>Angew. Chem. Int. Ed.</i> 2015 , 54, 12361
MoB	225	240		59	<i>Angew. Chem. Int. Ed.</i> 2012 , 51, 12703
Mo ₂ C	200	210		54	<i>Angew. Chem. Int. Ed.</i> 2012 , 51, 12703
FeP nanowires on carbon cloth	218				<i>ACS Catal.</i> 2014 , 4, 4065
WP nanorods on carbon cloth	120	175	280		<i>ACS Appl. Mater. Interf.</i> 2014 , 6, 21874
WN nanorods on carbon cloth	285	340	445	170	<i>Electrochim. Acta</i> 2015 , 154, 345
NiP ₂ nanosheets on carbon cloth	102	130	270	65	<i>Nanoscale</i> 2014 , 6, 13440
NiSe/Ni foam	96	130		120	<i>Angew. Chem. Int. Ed.</i> 2015 , 54, 9351
NiFe layered double hydroxide on Ni foam in 1.0 M NaOH	210	ca. 250			<i>Science</i> 2014 , 345, 1593
Co-MoS ₂	203	250	> 380	158	<i>Energy Environ. Sci.</i> , 2016 , 9, 2789
Ni/NiP	130	170		123.3	<i>Adv. Funct. Mater.</i> 2016 , 26, 3314.
Co-P nanocube	280	> 350		132.3	<i>Chem. Commun.</i> , 2016 , 52, 1633.

Table S3. Comparison of the electrocatalytic performance of the CoP NWs || oxidized CoP NWs electrode pair for two-electrode overall water splitting with that of reported non-precious metal electrocatalysts and precious metal electrocatalysts tested under similar conditions.

Electrode pair	V ₁₀ (V)	V ₂₀ (V)	V ₁₀₀ (V)	Durability test made	Reference
CoP NWs (cathode) oxidized CoP NWs (anode)	1.56	1.67	1.78	1000 h@20 mA cm ⁻² (ca. 1.68 V) ^a 1000 h@100 mA cm ⁻² (non-iR-corrected 2.05 V) ^a	This work
Co foam (CF)	1.89	1.94	2.06		This work
RuO ₂ Pt-C on CF	1.56	1.62	1.77		This work
EG/Co _{0.85} Se/NiFe-LDH	1.67	1.71	-	10 h@ 20 mA cm ⁻² (ca. 1.73 V) ^a	<i>Energy Environ. Sci.</i> , 2016 , 9, 478.
Ir-C Pt-C on EG	1.62	1.71	-	10 h@ 20 mA cm ⁻² (ca. 1.75 V) ^a	
c-CoSe ₂ /carbon cloth	1.63	1.8	-	2.8 h@1.7 V (ca. 12.5 mA cm ⁻²) ^b	<i>Adv. Mater.</i> , 2016 , 28, 7527-7532.
NiCoP/graphene	1.59	ca. 1.7		75h@1.59 V (10 mA cm ⁻²) ^b	<i>Adv. Funct. Mater.</i> 2016 , 26, 6785-6796.
Ni ₂ P on Ni foam	1.63	ca. 1.7		10 h@10 mA cm ⁻² (ca. 1.65 V) ^a	<i>Energy Environ. Sci.</i> 2015 , 8, 2347-2351.
Ni ₅ P ₄ on Ni foil	1.7	ca. 1.75			<i>Angew. Chem. Int. Ed.</i> 2015 , 54, 12361-12365.
Pt Pt	>1.8				
Co-P film	1.65	1.67		24 h@1.63 V (ca. 4 mA cm ⁻²) ^b	<i>Angew. Chem. Int. Ed.</i> 2015 , 54, 6251-6254.
IrO ₂ Pt-C	1.6	1.67		24 h@1.63 V (ca. 3.5 mA cm ⁻²) ^b	
Pt-C Pt-C	1.75	1.83			
IrO ₂ IrO ₂	>1.9	>1.9			
NiSe NWs on Ni foam	1.63	1.75	> 1.9 V	20 h @ 20 mA cm ⁻² (1.74 V) ^a	<i>Angew. Chem. Int. Ed.</i> 2015 , 54, 9351-9355.
Ni foam	1.93	>2.0			
Pt-C on Ni foam	1.67	1.75			
Ni(OH) ₂ /NiSe	1.78	-	-	2 h @ 5 mA cm ⁻² (1.8 V) ^a	<i>Chem. Mater.</i> , 2015 , 27, 5702-5711
Ni ₂ P/Ni/Ni foam	1.49	1.54	1.68	20 h@10 mA cm ⁻² (1.6 V) 20 h@20 mA cm ⁻² (1.65 V)	<i>ACS Catal.</i> 2016 , 6, 714-721
NiFe LDH on Ni foam in 1.0 M NaOH	1.7	1.78		10 h @1.8 V (40 mA cm ⁻² fell to 30)	<i>Science</i> 2014 , 345, 1593-1596.

				mA cm ⁻²) ^b	
Ni(OH) ₂ on Ni foam	1.8	1.9			
Ni foam	1.92	>2.0			
3.5 nm Pt on Ni foam	1.7	1.8			
Co-P film on Au foil	1.73			2 h @ 10 mA cm ⁻² (1.74 V) ^a	<i>RSC Adv.</i> 2015 , 5, 105814-105819.
FeP	1.69	1.75		14 h @ 10 mA cm ⁻² (1.69 V rose to 1.78 V) ^a	<i>Chem. Eur. J.</i> 2015 , 21, 18062 – 18067.
NiMo alloy	1.64	1.75		10 h @ 10 mA cm ⁻² (1.64 V) ^a	<i>J. Mater. Chem. A</i> 2015 , 3, 20056–20059.
RuO ₂ Pt-C both on Ti mesh	1.57	1.63			
CoSe film	1.65			27 h @ 10 mA cm ⁻² (1.65 V rose to 1.69 V) ^a	<i>Chem. Commun.</i> 2015 , 51, 16683–16686
CoO _x @CN on Ni foam	ca. 1.6		> 2.0 V	2.5 h @ 10 mA cm ⁻² (1.58 V rose to 1.7 V) ^a	<i>J. Am. Chem. Soc.</i> 2015 , 137, 2688–2694.
NiCo ₂ O ₄ Ni _{0.33} Co _{0.6} ₇ S ₂	1.72	1.8		20 h @ 1.65 V (5 mA cm ⁻² fell to 4.5 mA cm ⁻²) ^b	<i>Adv. Energy Mater.</i> 2015 , 5, 1402031.

V₁₀, V₂₀ and V₁₀₀ represent the required cell voltage to deliver current densities of 10, 20, 100 mA cm⁻² in the two-electrode electrolyzer, respectively. These cell voltage values are obtained from the polarization curves reported in this work of literature. Unless stated otherwise, the tests were made in 1.0 M KOH solution.

^aThe durability used the chronopotentiometry at the constant applied current density, recording the variation of the potential.

^bThe durability used the chronoamperometry at the constant applied potential, recording the change of the current density.

Estimation of the energy efficiency of water electrolyzers:

Water electrolysis involves the hydrogen evolution reaction (HER) on cathode and the oxygen evolution reaction (OER) on anode. The minimal cell voltage for water electrolysis in an open system, E_{cell}^0 , is given by the following equation under standard conditions (25 °C, 1 atm, P, T constant):

$$E_{cell}^0 = -\frac{\Delta G^0}{nF} \quad (3)$$

$$\text{or } \Delta G^0 = -nFE_{cell}^0 \quad (4)$$

where ΔG^0 is the change in the Gibbs free energy under standard conditions, n the number of electrons transferred, and F the Faradaic constant.

$$\Delta G^0 = \Delta H^0 - TR\Delta n - T\Delta S^0 \quad (5)$$

For the electrolysis of water, the standard reaction enthalpy is $\Delta H^0 = 285.8 \text{ kJ mol}^{-1}$, $\Delta n = 1.5$, ΔS^0 (H_2) = 130.6 J mol^{-1} , ΔS^0 (O_2) = 205.1 J mol^{-1} , ΔS^0 (H_2O) (l) = $70 \text{ J mol}^{-1} \text{ K}^{-1}$, $\Delta S^0_{\text{tot}} = 130.6 + \frac{1}{2} 205.1 - 70 = 163.14 \text{ J mol}^{-1} \text{ K}^{-1}$, and $\Delta G^0 = 237.2 \text{ kJ mol}^{-1}$. So the minimum cell voltage for an open cell is $E_{cell}^0 = -\Delta G^0/nF = 1.23 \text{ V}$, according to the equation (4).^[S8]

The maximum possible efficiency of an ideal open electrochemical cell is defined by the following equation:

$$\varepsilon_{\text{max}} = \frac{\Delta H^0}{\Delta G} = -\frac{\Delta H^0}{nFE_{cell}} \quad (6)$$

where E_{cell} is the cell voltage to drive water splitting at the current of I :

$$E_{cell} = E_{cell}^0 + IR + \Sigma\eta \quad (7)$$

where R is the total ohmic series resistance in the cell including resistance of external circuit, electrolyte, electrodes, and membrane materials (if any); $\Sigma\eta$ is the sum of overpotentials including the activation overpotential at the two electrodes and the concentration overpotential.

The splitting of water by electrolysis is an endothermic reaction with the enthalpy change defined as follows:

$$\Delta H^0 = \Delta G^0 + T\Delta S = -nFE_{cell}^0 + T\Delta S \quad (8)$$

where ΔG^0 supplies energy in the form of electricity and the rest, $T\Delta S$, by heat. In actual electrolysis, cell voltage is always higher than the theoretical voltage of electrolysis, namely reversible voltage $E_{cell}^0 = 1.23 \text{ V}$, and the difference is converted into heat. When the cell voltage reaches 1.48 V , all heat generated by overpotential and ohmic loss is used by the reaction, and at this voltage there is no heat generation or absorption to and from outside of the system (i.e., $\Delta S =$

0). Therefore, the cell voltage of 1.48 V is defined as “thermoneutral potential” where the cell does not heat or cool and all electric energy used for electrolysis is converted into heat content of evolved gas.^[S8, S9] This voltage is used as the standard of 100% efficiency. Since the current efficiency is almost 100% in water electrolysis, dividing 1.48 V by practical cell voltage (E_{cell}) will thus approximately give the energy efficiency of water electrolysis,^[S10, S11] according to equations (6) and (8):

$$\varepsilon \cong \frac{1.48 \text{ V}}{E_{\text{cell}}} \times 100\% \quad (9)$$

References

- [1] A. P. Grosvenor, S. D. Wik, R. G. Cavell and A. Mar, *Inorg. Chem.*, **2005**, 44, 8988–8998.
- [2] N. Jiang, B. You, M. Sheng and Y. Sun, *Angew. Chem. Int. Ed.*, 2015, 54, 6251–6254.
- [3] Y. Yang, H. Fei, G. Ruan and J. M. Tour, *Adv. Mater.*, **2015**, 27, 3175–3180.
- [4] X. Yang, A.-Y. Lu, Y. Zhu, M. N. Hedhili, S. Min, K.-W. Huang, Y. Han and L.-J. Li, *Nano Energy*, **2015**, 15, 634–641.
- [5] J. Tian, Q. Liu, A. M. Asiri and X. Sun, *J. Am. Chem. Soc.*, **2014**, 136, 7587–7590.
- [6] A. R. Kucernak and V. N. Sundaram, *J. Mater. Chem. A*, **2014**, 2, 17435–17445.
- [7] Z. Huang, Z. Chen, Z. Chen, C. Lv, M. G. Humphrey and C. Zhang, *Nano Energy*, **2014**, 373–382.
- [S8] E. Zoulias, E. Varkaraki and N. Lymberopoulos, A Review on Water Electrolysis. <http://www.cres.gr/kape/publications/papers/dimosieyseis/ydrogen/A%20REVIEW%20ON%20WATER%20ELECTROLYSIS.pdf>
- [S9] I. Abe, *Energy Carriers and Conversion Systems – Vol. 1 – Alkaline Water Electrolysis*, in Encyclopedia of Life Support Systems (EOLSS), Eolss Publishers, Paris, France [http://www.eolss.net/sample-chapters/c08/e3-13-03-02.pdf]

[S10] J. O. M. Bockris, B. E. Conway, E. Yeager and R. E. White, *Comprehensive Treatise of Electrochemistry: Electrochemical processing*, Springer US, New York, **1981**, page 14.

[S11] Z. Qi, *Proton Exchange Membrane Fuel Cells*, CRC Press, New York, **2013**, page 130.